Assessment of the Wet Season Precipitation in Central United States by the Regional Climate Simulation of WRFG Member in NARCCAP and Its Relationship with Large-scale Circulation Biases

Yating Zhao[1,2], Ming Xue[1,2*], Jing Jiang[1], Xiao-Ming Hu[2] and Anning Huang[1]
[1]School of Atmospheric Sciences, Nanjing University, Nanjing, China
[2]Center for Analysis and Prediction of Storms, and School of Meteorology, The University of Oklahoma, Norman, U.S.A

Corresponding author:
Ming Xue, CAPS, University of Oklahoma,
100 David Boren Blvd, Norman OK 73072.
mxue@ou.edu

ORCID of the authors：
Yating Zhao: 0000-0001-5268-9346
Ming Xue: 0000-0003-1976-3238
Jing Jiang: 0000-0002-3617-2424
Xiao-Ming Hu: 0000-0002-0769-5090
Anning Huang: 0000-0001-9872-440X

For Review Only

Abstract

Assessment of past-climate simulations of regional climate models (RCMs) is important for understanding the reliability of RCMs when used to project future regional climate. Here we assess the performance and discuss possible causes of biases of a WRF-based RCM with a grid spacing of 50 km, named WRFG, from the North American Regional Climate Change Assessment Program (NARCCAP) in simulating the wet season precipitation over the central United States for a period when observational data are available. The RCM reproduces key features of precipitation distribution characteristics during late spring to early summer, although it tends to underestimate the magnitude of precipitation. This dry bias is partly due to the model's lack of skill in simulating nocturnal precipitation related to the lack of eastward propagation of convective systems in simulation. Inaccuracy in reproducing large-scale circulation and environmental conditions is another contributing factor. The too weak simulated pressure gradient between the Rocky Mountains and the Gulf of Mexico results in weaker southerly winds in between, leading to less warm moist air transport from the Gulf to the central Great Plains. The simulated low-level horizontal convergence fields are less favorable than in NARR for upward motion and hence for convection development also. Therefore, careful examination of an RCM's deficiencies and the identification of the source of errors are important when using the RCM to project change of precipitation in future climate scenarios.

Keywords: NARCCAP; Central United States; Precipitation; Low-level jet; Large-scale environment; Diurnal variation

Article Highlights:

- The assessed climate model reproduces the key features of warm-season precipitation distribution but underestimates amount in central U.S.

For Review Only

- The lack of eastward propagation of convections from the Rockies into the Central Plains in simulations contributes to the dry bias
- Inaccuracies in large-scale circulation and environmental conditions from the Gulf to Great Plains also contributes to precipitation error

https://doi.org/10.1007/s00376-023-2353-x

For Review Only

1. Introduction

The North American Regional Climate Change Assessment Program (NARCCAP; Mearns et al., 2009) is a project that uses six regional climate models (RCMs) to produce dynamically downscaled regional climate simulations in order to investigate the uncertainties in projecting future climate under different climate change scenarios for impact research (http://www.narccap.ucar.edu/about/index.html). These RCMs are the Canadian Regional Climate Model (CRCM) (Caya and Laprise 1999), the Scripps Experimental Climate Prediction Center (ECPC) Regional Spectral Model (Juang et al., 1997), the Hadley Centre's regional model version 3 (HadRM3) (Pope et al., 2000), the fifth-generation of Pennsylvania State University-National Center for Atmospheric Research (NCAR) Mesoscale Model (MM5) (Grell et al., 1994), the Regional Climate Model version 3 (RegCM3) (Giorgi et al., 1993a,b), and the Weather Research and Forecasting model with the Grell-Devenyi cumulus scheme (WRFG) (Grell and Dévényi 2002). In the NARCCAP program, these RCMs are used to simulate regional climate for a historical period, and to downscale coupled atmosphere-ocean general circulation models forced with the A2 emission scenario (Nakicenvoic et al., 2000).

For Review Only

To understand the potential reliability of the RCMs for future climate simulations, it is necessary to assess their simulation performance for historical periods when observational data are available (Mearns et al., 2012; Pan et al., 2001; Giorgi, 2019), and to try to understand their simulation biases as much as possible. Towards this end, NARCCAP used NCEP-DOE Reanalysis-2 (R2) data (Kanamitsu et al., 2002) from 1979 to 2004 to drive the RCMs for the simulation of the historical climate of North America. By comparing all regional models within NARCCAP using various metrics, Mearns et al. (2012) provides a baseline evaluation indicating that all models can simulate some aspects of the climate reasonably well over the North America for the historical period. However, significant differences exist among the models that highlight uncertainties in modeling regional climate processes. To improve the understanding of the errors in the regional climate models, more analyses are needed.

Previous studies evaluated the NARCCAP RCM simulations for different geographic regions and on different aspects of simulation. Gutowski et al. (2010) found that for coastal California the models replicate well the frequency and magnitude of extreme monthly precipitation (top 10% of monthly precipitation), and the associated circulation anomaly in the cold half year for the period 1982-1999. The models reproduce well the interannual variability of the occurrence of the extreme. For the upper Mississippi River basin, Kawazoe and Gutowski (2013) found all models generally reproduce the precipitation intensity spectra seen in observations well, with a small tendency toward producing overly strong precipitation at high-intensity thresholds. Wang et al. (2009) evaluated the precipitation climatology of the intermountain region of western United States between the Cascade-Sierra range and the Rocky Mountains and found systematic biases with six regional climate models in NARCCAP. The simulated winter precipitation is too large and the simulated annual cycles are too strong. Leung and Qian (2009) pointed out that during the cold season, the WRF-member simulation in NARCCAP realistically captured the amount and spatial distribution of mean precipitation intensity, extreme (95th percentile) precipitation, and the precipitation/temperature anomalies of all the atmospheric river events between 1980-1999 in the topographically diverse western U.S.

For the central United States, the broad expanse of flat land between the Rocky Mountains and Mississippi River depends on summer rainfall for its extensive agricultural land use. Thus, the processes contributing to precipitation (Carbone and Tuttle 2008; Weckwerth and Romatschke

For Review Only

2019; Trier et al. 2020) and the question of how well numerical models simulate precipitation in the past and predict possible changes in the future have attracted great research interest (Gutowski et al., 2010; Harding and Snyder 2014). Precipitation across this region is difficult to simulate with accuracy when using global climate models (GCM) with coarse resolutions (Klein et al., 2006; Harding et al., 2013).

Dynamically downscaling the GCM outputs by using high resolution RCMs can reduce the simulation bias (Liang et al., 2006; Dickinson et al., 1989). However, the RCMs show conspicuous differences in simulating central U.S. warm season rainfall. Some of them oversimulate precipitation over the central U.S. (Bukovsky and Karoly 2009; Qiao and Liang 2015; Kawazoe and Gutowski 2018). Some of the others undersimulate precipitation in this region (Harding et al., 2013; Gao et al., 2017; Tian et al., 2017; Harris and Lin 2014; Lee et al., 2007a; Kim et al., 2013). Sun et al. (2016) found that dynamic downscaling simulations they produced at both 4-km and 25-km grid spacings share similar low precipitation bias over the central U.S. The bias appears linked to circulation biases in the simulations. Hu et al. (2018) also noticed significant warm-season precipitation and circulation biases in their dynamically downscaled simulations. Spectral nudging was found to help alleviate the precipitation biases by reducing circulation biases. Kawazoe and Gutowski (2018) found that some RCMs undersimulate the intensity of strong widespread precipitation events in the upper Mississippi region and suggested the need for deeper look into the connection between the large-scale circulation and precipitation. Overall, the skill of RCMs in simulating precipitation over the central U.S., and the sources of the precipitation biases still require more detailed assessment and analyses. In NARCCAP, there are similar warm season precipitation biases among most RCM members; that is, dry bias over the central U.S., and wet bias over the Rocky Mountains region and the southeast coast. The central U.S. dry bias in the

https://mc03.manuscriptcentral.com/aasiap

WRFG member is about the largest among the NARCCAP RCM members (Mearns et al., 2012) and the WRF model is among the mostly widely used models for weather prediction and for regional climate simulations (Tapiador et al., 2020). For these reasons, this paper focuses on the WRFG member of NARCCAP simulations, and tries to better understand its behaviors for historical simulation. Specifically, we examine a 19 year period from 1986 through 2004, and assess WRFG's performances in reproducing the mean behaviors and diurnal variation of wet season precipitation over the central U.S. (in the red box shown in Fig. 1), part of the entire model domain that covers the conterminous United States and most of Canada. We further investigate the relationship between precipitation biases and circulation simulation biases, in an attempt to better understand the physical causes of the precipitation bias.

The rest of this paper is arranged as follows. The data sources are described in Section 2. In Section 3, we assess how well WRFG simulates precipitation in the wet season over the Great Plains region of the central U.S. In section 4, the possible relationship between simulated precipitation, associated circulations, and their biases are discussed. Section 5 summarizes the results and presents conclusions.

For Review Only

2. Data

2.1. Reference data

We use the monthly precipitation data from Parameter-elevation Regressions on Independent Slopes Model (PRISM) dataset (Daly et al., 1994) as one of the precipitation reference data. We analyze the data during the period from 1986 to 2004 to be consistent with the WRFG simulation. The PRISM monthly mean precipitation dataset (available at http://prism.oregonstate.edu) covering the contiguous U.S. (CONUS), starting in January 1895, is produced by gathering climate observations from a wide range of monitoring networks, applying sophisticated quality control measures. We use it in this study because of its high spatial resolution (4 km grid spacing), the use of sophisticated elevation correction scheme and inclusion of data from around 8000 stations. More important is its long period of data coverage; the dataset has been used in previous studies evaluating the performance of RCMs (e.g., Hu et al., 2018).

The 4-km NCEP Stage IV precipitation dataset (Lin and Mitchell 2005) is also used for analysis and comparison (available at https://www.emc.ncep.noaa.gov/mmb/ylin/pcpanl/stage4/). It is mosaicked from regional multi-sensor (radar and gauges) precipitation analyses covering the period from 2002 onward, and the data up to 2015 are used in this study. The high spatial (4-km grid spacing) and hourly temporal resolutions of the dataset enable the investigation of diurnal variability of precipitation. The Stage IV product is currently the only long-running operational product that provides high-resolution radar-based precipitation estimates over the CONUS and especially the hourly temporal resolution and thus is used in many studies on precipitation (Nelson et al., 2016). Unfortunately, there is little overlap between the available period of Stage IV data (from 2002 onward) and the WRFG simulation period (1986 – 2004). Studies have found that the diurnal cycle in summer precipitation has small year-to-year variation (Dai et al., 1999; Liang et al., 2004), particularly in terms of the diurnal phase. Due to the lack of high spatial and temporal resolution precipitation data set over the 1986-2004 period that WRFG is run over, for the purposes of evaluating precipitation diurnal variations and spatial propagataion, we will use the Stage IV data in the 2002-2015 period as a substitution, assuming this aspect, especially the diurnal phase, of precipitation over the central U.S. is similar between the two periods. When the Stage IV data are used for comparison, less emphasis should be placed on precipitation intensity because of possible year-to-year variability.

For Review Only

The NCEP North American Regional Reanalysis (NARR; Mesinger et al., 2006), a regional reanalysis over North America (available at https://www.esrl.noaa.gov/psd/data/gridded/data.narr.html) is used to evaluate the WRFG-simulated atmospheric fields including air temperature, wind, moisture, and geopotential height. The NARR dataset covers 1979 through present. The then-operational NCEP Eta Model with 32 km horizontal grid spacing and 45 layers was used together with the Regional Data Assimilation System (RDAS) to assimilate precipitation along with other observations. The improvements in the model and data assimilation systems resulted in a dataset with better accuracy of temperature, winds and precipitation analyses compared to the NCEP-DOE Global Reanalysis 2 (Mesinger et al., 2006). We use the NARR data available 8 times daily on 29 vertical levels from 1986 to 2004 for the evaluation of WRFG-simulated atmospheric states. We note that the ERA5 (Lavers et al., 2022) global reanalysis dataset is available at hourly intervals but the reanalysis does not assimilate rain-guage precipiattion data.

2.2. WRFG RCM simulation output

As mentioned earlier, the RCM simulation evaluated in this study is the NARCCAP member using WRF model with Grell-Devenyi cumulus parameterization scheme (Mearns et al., 2009). The WRF modeling system is community supported and is widely used throughout the world for a variety of weather and climate applications (Tapiador et al., 2020). However, the WRFG member in NARCCAP has about the largest simulation bias in the region of our research interest which deems a detailed investigation necessary. WRF is a fully compressible, non-hydrostatic model with terrain-following mass-based vertical coordinates and contains a large collection of physical parameterization schemes that can be used to build regional climate simulation systems

For Review Only

(Skamarock et al., 2005). In NARCCAP, a WRF member named WRFP was initially run by the Pacific Northwest National Lab (PNNL) using the Kain-Fritsch cumulus parameterization scheme. It was later superseded by a new run using the Grell-Devenyi cumulus scheme that improved the reproduction of temperature and precipitation. This WRFG member is examined in this study.

For NARCCAP, WRF was run at a 50-km horizontal grid spacing with 35 vertical levels over a domain covering the CONUS and most of Canada. Other model physics include the Grell-Devenyi cumulus scheme, the WRF single-moment 5-categry (WSM5) microphysics scheme, CAM3 shortwave and longwave radiation scheme, Yonsei University (YSU) planetary boundary layer scheme, and the NOAH land surface model. The full name of this run is WRFG-NCEP, where NCEP indicates the use of NCEP global reanalysis for initial and lateral boundary forcing. The full length of simulation is from 1979 to 2004. For this study we examine a 19 year period from 1986 to 2004, which avoids the spin up period and is still long enough for statistical evaluation (given our focus on the mean behaviors of precipitation simulation and its diurnal variation). Considering that WRF has many options for physics parameterizations, our evaluation in this paper is strictly speaking valid only for the particular configurations used. However, some of the behaviors may be common to other physics options or even other models.

3. Assessment of wet season precipitation simulated by WRFG in central U.S.

The climate in central U.S. has strong seasonal variability. In this region, more than half of total annual precipitation occurs during the wet season, which includes late spring and early summer (Higgins et al., 1997; Mearns et al., 2012; Wallace, 1975). In view of this, we assess the simulated precipitation in May, June, and July. To reduce differences in the precipitation intensity purely because of grid resolution difference, we regrid the ~4 km PRISM and Stage IV

https://mc03.manuscriptcentral.com/aasiap

For Review Only

precipitation data to the ~50 km WRFG grid by using NCL ESMF_regrid function with the "conserve" interpolation option. This method tries to preserve the integral value of the interpolated fields and is therefore a preferred choice for mapping high-resolution precipitation to a lower-resolution grid. As seen in Fig. 2a, the average daily mean precipitation intensity in the PRISM data in May is larger than 2 mm day^{-1} in central U.S. with the highest intensity of more than 4.5 mm day^{-1} located in the bordering regions of Oklahoma-Kansas and Arkansas-Missouri. May and June are similar in the distribution precipitation pattern but are different in intensity. In June, the rainfall maximum is ~ 4 mm day^{-1}, weaker than in May (Fig. 2b). In July (Fig. 2c), the rainfall maximum is located at the northeast of Kansas, exceeding ~ 4 mm day^{-1} over only a small area. In May and June, regions with 3 mm day^{-1} average precipitation extend to the Gulf coast, but in July, such regions move northward up to northeastern Oklahoma.

In comparison, the WRFG-simulated precipitation is much weaker in all three months (Fig. 2d.-2f). The WRFG model can roughly reproduce the principal precipitation distribution characteristics over CONUS, that is, strong rainfall in the central and east parts of CONUS and little rainfall in the western part of the country from May to July. It however significantly underestimates the daily mean precipitation intensity in regions of the Gulf of Mexico coast in May (Fig. 2d) and the entire central U.S. in July (Fig. 2f).

In May (Fig. 2d), daily mean precipitation of over 3 mm day^{-1} is mostly captured over the eastern half of CONUS, but the intensity does not reach 4 mm day^{-1} while the observed maximum is more than 4.5 mm day^{-1} (Fig. 2a). The western edge of heavier precipitation also deviates to the east by about 2° longitude or about 200 km (Fig. 2d), and the precipitation within a zone of about 200 km width along the gulf coast is also too weak. The general pattern and intensity of precipitation on the western half of CONUS agree better with observations (Fig. 2a and 2d).

For Review Only

In June, the simulated dry bias is more significant; it misses all heavy precipitation over 4.5 mm day^{-1} along the Gulf coast and significantly under-predicts precipitation west of Mississippi River especially over the central and southern Great Plains (Fig. 2e). In July, the dry bias is even more severe. Nowhere over the central U.S. does the daily mean precipitation exceed 2.6 mm day^{-1} (Fig. 2f). Over the northern Plains it is about half of the observed amount. Over central Oklahoma, a minimum of less than 1.1 mm day^{-1} is simulated while the observed amount is around 2.2 mm day^{-1}. The warm season simulation dry bias is consistent with earlier area-averaged precipitation assessments over a similar region in the central U.S. (Mearns et al., 2012; Kawazoe and Gutowski 2018).

The diurnal variations of mean precipitation intensity averaged over the Central U.S. within the red polygon in Fig. 1 are shown in Fig. 3 for the Stage IV data for 2002-2015 (solid lines) and the WRFG simulation for 1986-2004 (dashed line) for May, June and July. The mean precipitation intensities in Stage IV data are obtained by averaging hourly accumulated precipitation over the previous three hours to the times labeled in the figure. The precipitation intensity in WRFG is given as the average of instaneous rainfall rates over the previous 3 hours. Here, as mentioned earlier, we assume the general stationarity of the precipitation propagation characteristics and diurnal cycles over the past few decades, which is supported by earlier studies.

The general oscillations of diurnal variations in precipitation are reasonably captured in the WRFG simulation, agreeing with previous studies that examined very heavy precipitation events in a similar region (Kawazoe and Gutowski 2018). However, the amounts and amplitudes are mostly smaller than observed values, with the relative errors being the smallest in May and largest in July (Fig. 3) in the region we focus on. The peaks of precipitation intensity in the Stage IV data appear at mid-night in May and at 3 am local time in June and July while in the model simulation

For Review Only

they all appear at mid-night. A pronounced minimum appears at the local noon when the intensity is mostly less than half of the peak. The precipitation diurnal variation patterns for May, June, and July are similar, but the amplitudes of oscillation are different. For May and June, the maximum is about 5 mm day^{-1} while the minimum value is between 2.4 and 2.6 mm day^{-1} in the observations. For July, the variation is between 1.9 and 3.7 mm day^{-1}. These results are consistent with previous studies (e.g. Lee et al., 2007a; Carbone et al., 2002; Dai et al., 1999; Higgins et al., 1997; Liang et al., 2004; Riley et al., 1987; Tian et al., 2005; Wallace 1975) finding that the summer precipitation over the central U.S. has unique diurnal variations. Nocturnal precipitation accounts for the vast majority of total warm-season precipitation in this region (Chen et al., 2009; Higgins et al., 1997; Jiang et al., 2006).

The model-simulated maximum precipitation intensity in May is about 1 mm day^{-1} smaller than that in Stage IV data. In July, the simulated value is ~ 2 mm day^{-1}, about half of the observed 3.8 mm day^{-1} in the early morning. Also the observed peak is at 3 am while the simulated amount at midnight is slightly higher. In May and June, both absolute and relative errors at noon time are relatively small, but those at midnight peak are much larger. In July, the errors are large in both day and night times. The above results are consistent with the monthly mean precipitation intensity comparisons with PRISM data as presented in Fig. 2, supporting the precipitation stationarity assumption. Overall, the above results also suggest that the primary deficiency of the model in simulating the wet season precipitation over the central Plains is with its lack of skill in simulating the nocturnal precipitation. Since the largest error occurs in July, we will focus in the rest of this paper on July, and will pay most attention to night precipitation, in order to gain understanding on the nature and cause of such error.

For Review Only

4. Physical processes associated with the dry bias in central U.S.

The night precipitation maximum over the central Plains has been attributed to the eastward propagation of convective systems initiated in the afternoon over the Rocky Mountain regions that arrive at the central Plains at night (e.g., Jiang et al., 2006; Carbone and Tuttle 2008; Geerts et al. 2017; Weckwerth and Romatschke 2019), and to locally initiated mesoscale convective systems by nocturnal low-level jet (Blackadar, 1957; Bleeker and Andre, 1951; Hering and Borden, 1962; Pitchford and London, 1962; Geerts et al. 2017). In the next two sections, we will examine how well WRFG simulates the eastward propagation of precipitation systems, and the synoptic and mesoscale circulations that can affect local forcing to convective systems at night.

4.1 Eastward propagation of convective systems from the Rocky Mountains

The 3-hourly Stage IV precipitation averged over years 2002-2015 are shown in Fig. 4. It is seen that in the afternoon (between 12 and 15 CST, Fig. 4h), convective systems are clearly evident over the Rocky Mountain regions of Colorado and New Mexico. Such convection should be due to daytime heating of the elevated terrain. Over the next few hours (between 15 and 21 CST, Figs. 4a-b), the main precipitation zone is found to shift eastward, being located in eastern Colorado between 18 and 21 CST, and over the eastern Colorado and New Mexico Borders by 00 CST (Fig. 4c). Based on a 12-year climatology, Carbone and Tuttle (2008) found that propagating precipitation episodes, i.e., precipitating systems propagating into the region from the upstream, contributed 60% of the summer rainfall to the central United States. Weckwerth and Romatschke (2019) examined cases that occurred during the Plains Elevated Convection At Night (PECAN) field campaign (Geerts et al. 2017), and found that 70% of the Great Plains precipitation was caused by episodes that formed outside of the PECAN domain (centered over Kansas) and propagated into the region. Mountain-initiated storms formed primarily in the afternoon and the

For Review Only

surviving ones propagated eastward, grew upscale, and contributed 27% of the precipitation in the plains (Weckwerth and Romatschke 2019). The fact that the precipitation zone shifts continuously eastward with time as shown in Fig, 4 suggests that the propagation of convection storms initiated over the Rocky Mountains into the central Plains while growing upscale is responsive for at least part of the night time precipitation over the Plains, and this is even more evidence when examining hourly precipitation (not shown).

By 03 CST, most of the precipitation is over the central part of the Great Plains (Fig. 4d) and by early morning it is mostly located over the eastern borders of Oklahoma, Kansas and into Iowa and further north (Fig. 4e). Between 00 and 06 CST, precipitation is mainly found over the central part of the Central Great Plains. Such precipitation is believed to linked to the Great Plains nocturnal low-level jet, whose northern terminus is located in the Central Great Plains during this period (e.g., Weckwerth and Romatschke 2019; Trier et al. 2020), and the merger of the systems propagating into the region with locally-initiated precipitation would also play a role, as documented in Weckwerth and Romatschke (2019) . At 03 CST (Fig. 4d), the precipitation budget box used in Fig. 3 (see Fig. 1) is filled with both convective systems that have propagated into the region, and systems that initiated locally; this would explain the precipitation peak at 03 CST in the region seen in Fig. 3.

Over the three hours following 06 CST, the main precipitation zone continues to shift eastward, to a north-south axis through central Arkansas by 09 CST. Such shift should be related to the eastward propagation of convective systems (e.g., Carbone and Tuttle 2008). The systems in Central Plains weakens significantly between 06 and 09 CST, and are mostly dissipated after 09 CST (Fig. 4g). At the 12 CST noon, the precipitation over the Central U.S. is indeed at a minimum (Fig. 4g) while by mid-afternoon (Fig. 4h), new convection has developed, over the Rockies, the

For Review Only

eastern part of U.S. and over parts of the Central Plains (Fig. 4h). Most of the heavy precipitation along the Gulf coast seen in the PRISM data (Fig. 2) is clearly from afternoon convection (Fig. 4h). The propagation of convective systems across the Central Plains overnight discussed above agrees with previous studies that some of the convective storms initiated over the Rockies in the afternoon can propagate eastward and become organized, creating coherent structures in precipitation Hovmoller diagrams (Carbone et al., 2002; Liang 2004; Jiang et al., 2006). The eastward propagation of organized convective systems is indeed an important contributor to the nocturnal precipitation over the Great Plains (Jiang et al., 2006; Weckwerth and Romatschke 2019). Thus, whether the model can reasonably reproduce the eastward propagation of convective systems initiated over the Rockies would affect its performance in simulating the timing, distribution, and intensity of the central U.S. nighttime precipitation.

The WRFG-simulated 3-hourly precipitation intensities averaged over the 1986-2004 simulation period, are plotted in Fig. 5. The difference in the averaging periods is due to the difference in data availability, as discussed earlier. It should be pointed out that due to this difference, the comparison between the precipitation intensities among the two datasets should be viewed with caution, due to possible year-to-year variability in precipitation amount. For example, certain years can be wetter than other years. The emphasis of the comparisons in Figs. 3 through 6 should be placed on the diurnal temporal variations and spatial propogation, and less so on intensity. For these comparisons, we are effectively assuming the general stationarity of the precipitation propagation and diurnal variation characteristics over the past few decades, which is supported by earlier studies indicating that the diurnal cycle in summer precipitation has small year-to-year variation (Dai et al., 1999; Liang et al., 2004).

Figure 5 shows that there are clear pattern differences between the simulation and Stage IV

For Review Only

data. In the afternoon (Fig. 5h), precipitation develops over the Colorado and New Mexico mountains, due to convection from thermal forcing. However, such convection fails to organize into long-lived MCSs and dissipates before moving much farther eastward onto the Plains. (Fig. 5a-d). Over the Great Plains, there is scattered precipitation from the afternoon to the next early morning (Fig. 5a-f) that appears to be strongest around midnight (Fig. 5c). The weaker simulated precipitation over north-central Great Plains at midnight (Fig. 5c) roughly corresponds to the locally developed precipitation in the observations (Fig. 4c). The precipitation over the Great Plains weakens after midnight and becomes mostly dissipated by the next noon (Fig. 5d-f).

The difference in the propagation characteristics is further illustrated by Hovmoller diagrams of precipitation averaged over the 35°N-45°N latitude band (the southern and northern boundaries of the red budget box in Fig. 1) and normalized by daily average precipitation (Fig. 6). In the Stage IV data (Fig. 6a), precipitation first occurs in the afternoon after 14 CST, over the Rocky Mountains west of 105°W, then starts to move eastward from the mountainous region afterwards at a speed of about 10° longitude over 12 hours. The most intense precipitation reaches 100°W around midnight while the eastern edge has reached 95°W. The precipitation continues to move eastward and reaches 90°W at around 06 CST at its leading edge (Fig. 6a). The rate of eastward propagation appears to accelerate somewhat between 03 and 06 CST; this should be a result of locally developing precipitation after 03 CST to the east (around 95°W) instead of being all caused by eastward propagation. The precipitation is weakest between 09 and 15 CST. All of these results are consistent with the overall diurnal variations of precipitation over the Central Plains seen earlier.

Within the WRFG simulation, between the 100°W and 95°W longitude zone, precipitation

For Review Only

maximum is found between 18 CST and 00 CST (Fig. 6b), roughly 3 hours earlier than observed and the propagating precipitiation is also displaced eastward by about 5° (Fig. 6a). West of 105°W, the afternoon precipitation does not show much sign of eastward propagation and the most intense precipitation remains west of 109°W (Fig. 6b). In fact, between 105°W and 100°W, and from 21 CST to 03 CST, there appears to be a precipitation 'trough', suggesting in another way the lack of eastward propagation of precipitation across the region into the Central Plains. The stronger precipitation east of 100°W between 18 CST and 00 CST appears to be locally initiated and it does show signs of eastward propagation after formation (Fig. 6b). The above results clearly show that WRFG fails to reproduce the eastward propagation of convection that develops in the afternoon over the Rockies, that based on the Stage IV data and other earlier studies are important contributors to the nighttime and overall precipitation over the Central Plains.

The anomaly in simulating eastward propagation of convective systems has also been reported in other regional climate simulations (Klein et al., 2006; Lee et al., 2007b; Sun et al., 2016; Hu et al., 2018). The difficulty for models that rely on cumulus parameterization to produce most convective precipitation has been pointed out in previous research (e.g., Brockhaus et al., 2008; Dai et al., 1999; Gochis et al., 2002; Harding et al., 2013; Klein et al., 2006; Molinari and Dudek, 1992; Weisman et al., 1997). Models run at convection-allowing/resolving resolutions are significantly better at reproducing propagation of mesoscale convective systems (e.g., Davis et al. 2003; Clark et al., 2009; Hu et al., 2018; Kwon and Hong, 2017; Lim et al., 2014; Sun et al., 2016). Given that many climate simulations will continue to use convection-parameterizing resolutions, especially for global climate models (Gutowski et al., 2020), this problem remains important, especially for regions where precipitation is significantly affected by propagating systems. A reasonable solution has to be found for future regional climate simulations at convection-

For Review Only

parameterizing resolutions, as far as water cycles are concerned. The defect of the model in simulating the eastward propagation process at least partly contributes to its dry bias in simulating the central U.S. precipitation.

4.2. Large-scale atmospheric circulation and environmental conditions

Mesoscale convective systems (MCSs) most often develop in favorable large-scale environments with adequate water vapor, atmospheric instability, and effective uplift (Houze, 2004; Loriaux et al., 2016). Thus, how well a regional climate model simulates the large-scale environmental conditions that trigger and forcing convection affects its performance simulating precipitation. Hence, we evaluate the regional atmospheric circulation and environmental conditions simulated by WRFG and hope to gain further insights into its precipitation simulation error. Because the main precipitation error occurs in the early morning hours, in the rest of this section, we will focus on circulations and other atmospheric conditions in the early morning, in particular at 06 CST (1200 UTC) when reanalysis data are available.

4.2.1. Large-scale atmospheric circulation

Figure 7 shows the geopotential height and horizontal wind field on 850 hPa level in the early morning at 6 CST of July averaged over 1986-2004 in NARR reanalysis data (Fig. 7a) and WRFG simulation (Fig. 7b). The Bermuda high, a semi-permanent, subtropical high pressure in the North Atlantic Ocean off the east coast of North America is closely linked to the regional climate of the central and east parts of U.S. (Diem, 2006; Katz et al., 2003; Henderson and Vega, 1996; Li et al., 2011; Ortegren et al., 2011; Stahle and Cleaveland, 1992). If using the 1560 gpm contour at 850 hPa to represent the boundary of the Bermuda High following Li et al. (2011), the Bermuda High in WRFG appears narrower in its north-south extent, and its east-west ridge axis is located further north, from the observed ~25°N to simulated ~ 31°N. This northward displacement means that

For Review Only

there is stronger easterly and weaker southerly component in the onshore flow towards Texas from the Gulf of Mexico in WRFG than in the observation, potentially transporting less moisture from the Gulf into the central U.S. On the northwest side of the Bermuda High, the southerly flows appear to extend further north in NARR than in WRFG, again potentially bringing more moisture and high-instability air into the Central U.S. Apart of these potentially important differences in details, overall, the circulation pattern over CONUS is reproduced reasonably well.

To reveal the relationship between the Great Plains precipitation and the low-level atmospheric circulation, we calculate the correlation coefficient of the July precipitation intensity within the red budget box of Fig. 1 (blue box in Fig. 8) and the 850 hPa geopotential height at individual grid points, and the correlation coefficients between precipitation intensity and horizontal wind components at the 850 hPa level (Fig. 8a) using NARR reanalysis. For the wind components, the two correlation coefficients are plotted in the form of vectors, so that a long northeastward-pointing vector means large positive correlations with both components. Figure 8 shows that the precipitation intensity within our budget box is negatively correlated to the 850 hPa height in a zone stretching from southwestern Texas through southwestern Iowa, and positively correlated with the 850 hPa height in the coast region of eastern Gulf of Mexico, with the maximum located at the Alabama coast. Such a correlation pattern clearly indicates that the precipitation in our budget region is positively correlated with the geopotential height gradient at the northwestern perimeter of Bermuda High, which is directly linked to the geostrophic wind speed along the perimeter. This is confirmed by the correlation coefficient vectors shown in Fig. 8a. Stronger southwesterly wind at the 850 hPa level between the locations with positive and negative height correlation coefficients enhances precipitation in the Central U.S. The southwesterly winds, making up a synoptic low-level jet (LLJ) at the perimeter of the Bermuda High, transport warm,

For Review Only

moist marine air from the Gulf of Mexico to the Great Plains and the Midwest region and have great impact on the precipitation distribution and intensity over this region (Higgins et al., 1997; Zhu and Liang 2007, 2005a; Helfand and Schubert 1995; Wang and Chen 2009). Consequently, error in predicting such flows would lead to error in precipitation simulation in the region.

The difference fields between the WRFG simulation and the NARR reanalysis in 850 hPa geopotential height and winds (Fig. 8b) show a 'horse saddle' pattern, with two high anomaly centers located in western Texas (that probably extends all the way over northwest U.S.) and eastern U.S., and two low anomaly centers over Kansas and the Gulf of Mexico. Such pattern corresponds to too weak subtropical high over the Gulf, and too high pressure over western Texas – leading to too weak east-west pressure gradient over southern Texas, the path of warm moist air from the Gulf into the Central Great Plain. Related to this pattern, the flows near the southern Texas Gulf coast show northerly anomaly what would act to reduce onshore moisture transport (Fig. 8b). Further, there is northerly wind anomaly in west Texas and southeast wind anomaly in northeast Texas. These differences are partly the result of eastward shift of southerly LLJ, leading to possibly less convective storm initiation in the western part of Texas and Oklahoma. The suggested negative biases in warm moist air transport from the Gulf into Central Great Plains can explain to some extent the dry bias in WRFG over Central U.S. Further north, the height anomaly pattern implies higher pressure gradient and stronger southerly flows in WRFG at 850 hPa over the southeastern part of our budget box in WRFG. Such flow anomaly appears to have, however, mostly originated from the southeast coastal regions rather than from the ocean in the Gulf. Also, even if they transport more moisture, they will mainly contribute to precipitation in the mid-west region outside of our budget box.

Figure 9 shows the vertical cross-sections of mean air temperature and geopotential height at

For Review Only

6 CST in July with their horizontal means removed, along the northwest-southeast slope in Texas (denoted as the brown line in Fig. 8b). The topography decreases from west Texas to the coastal region. In the lower level of the troposphere, there is a warm low pressure system over the plateau and a cold high pressure system over the gulf coastal plain. The land surface absorbing solar radiation acts as an elevated heat source for the atmosphere. The horizontal thermal contrast (Fig. 9a) partly leads to the horizontal pressure gradient (by lowering pressure on the west side, Fig. 9b), and southerly wind over Texas (Fig. 10a) in the lower troposphere in the NARR reanalysis. The difference fields between WRFG simulation and the NARR reanalysis in Fig. 9c. clearly show cold bias of temperature within about 1 km above the land surface in simulation. At the 825 hPa level, the along-slope thermal contrast is one-third smaller in simulation. Correspondingly, the horizontal geopotential height gradient along the slope is about 50% smaller in simulation than in NARR reanalysis (Fig. 9d). These may be one of the reasons for the simulation bias in the low level southerly winds (Fig. 10).

In the NARR reanalysis data, the time-averaged southerly LLJ is in the lower troposphere over the sloping terrain from the New Mexico Plateau to the plains in central and eastern Texas (Fig. 10a). The climatological average maximum meridional wind speed of the jet is larger than 8 m s^{-1} at the height of about 1 km above the ground. It can be decomposed into two components including geostrophic wind and ageostrophic wind. The geostrophic meridional component is southerly from the surface to the middle troposphere (Fig. 10b). At the height of LLJ, at about 875 hPa over the plateau and about 925 hPa over the Plains (over these regions, these heights are within the planetary boundary layer, and the jet is boundary layer LLJ that reaches peak intensity in early morning and the boundary layer inertial oscillation is believed to be the primary cause, Blackadar, 1957), the geostrophic meridional wind is about 6 m s^{-1}. The ageostrophic meridional component

For Review Only

at the same height is weaker, which is about 3 m s^{-1}. The difference fields between WRFG and NARR show that the simulated meridional wind of LLJ is about 2 m s^{-1} weaker, and the core of LLJ is shifted downward compared to NARR (Fig. 10d). These results echo and enrich research that reported WRFG tends to underestimate the warm season southerly LLJ frequency, speed and elevation at the rawinsonde locations in the central plains (Tang et al., 2016). They highlighted the need to further examine the differences in the jet formation mechanisms. Our research indicates this simulation bias can be at least partly attributed to the weaker southerly geostrophic wind component (Fig. 10e). At the level of LLJ core, there is clear northerly anomaly in geostrophic winds (Fig. 10e), which is likely related to the error in land surface processes in WRFG that affects the east-west geopotential height gradient. The simulated ageostrophic southerly wind at the level of LLJ core is weaker (Fig. 10f). The downward shift of the LLJ core is related to the near ground southerly anomaly in ageostrophic winds. This suggests possible error sources in boundary layer parameterization, because of the key role of boundary layer inertial oscillation in producing the boundary layer nocturnal LLJ (Blackadar 1957; Xue et al., 2018; Huang et al., 2022).

For Review Only

4.2.2. Environmental conditions

The LLJ simulation biases discussed can cause biases in moisture transport toward the Central Plains leading to errors in precipitation simulation over Central U.S. The NARR reanalysis (Fig. 11a) shows clearly there exists a water vapor transport channel over the east-west sloping terrain, transporting moisture northward. The moisture transport channel is roughly located at the level of the boundary layer LLJ, which is about 1 km above the slope. The maximum meridional moisture transport is at ~ 875 hPa over the plateau and ~950 hPa level over the Plains. In WRFG, the low-level water vapor transported through this cross-section is about 25% lower than in NARR based on the difference field (Fig. 11b). Considering that a significant part of the convective systems in central U.S. have updraft source levels at the low levels (Weckwerth et al., 2004), we use vertically integrated moisture flux convergence from surface to 700 hPa to determine the favorable locations for convection development (Banacos and Schultz 2005). In NARR reanalysis, the water vapor from the Gulf of Mexico travels through Texas then converges in the downstream regions over Oklahoma, Arkansas, Missouri, Kansas, and southern Iowa in July (Fig. 12a). While in WRFG, the water vapor convergence in Oklahoma and Kansas is smaller; there is little moisture convergence in Iowa (Fig. 12b). This can contribute to the dry bias in the simulation.

The atmospheric circulation transports not only moisture but also energy from subtropical regions to higher latitudes by the LLJ carrying high-energy and high-entropy air at the low levels which can rise under appropriate vertical lifting in the mid-latitudes and thereby affecting the generation and maintenance of mesoscale convection (Pauluis et al., 2008). The northward energy transport by the warm moist air can be approximately expressed as moist enthalpy transport. The moist enthalpy is defined by

$$H = C_p T + L q_v \ , \qquad (1)$$

where C_p is the heat capacity of the dry air at constant pressure, T the temperature, q_v the specific humidity, L the latent heat of vaporization of liquid water. The northward moist enthalpy transport flux is

$$vH = vC_p T + vLq_v \ , \qquad (2)$$

where v is the meridional wind component. The northward moist enthalpy transport consists of meridional sensible heat flux and latent heat flux. The NARR reanalysis data show that the maximum sensible heat is transported northward in lower troposphere, in which the core of sensible heat flux is located at about 1 km above the slope ground surface, apparently because of the boundary layer LLJ (Fig. 13a). The maximum center is mostly located west of 100°W. In

For Review Only

WRFG, less sensible heat is transported northward (Fig. 13b), and the maximum center is dislocated eastward to ~97°W at ~925hPa level. In NARR reanalysis, the northward latent heat flux has almost identical location and pattern in the vertical cross section as the sensible heat flux, apparently due to the LLJ again (Fig. 13c). The simulated northward latent heat flux is also weaker and its maximum location shifted eastward (Fig. 13d). In general, lower amounts of latent heat and sensible heat are transported northward from the Gulf to the Great Plains in the WRFG simulation than in NARR and the maximum transport channel is shifted eastward by several degrees. Less energy transport implies weaker convection and less precipitation in the simulation.

The lifting of air parcels to their level of free convection is a necessary ingredient of deep convection (Houze, 2004; Loriaux et al., 2016). In the Central U.S., the low-level lifting forcing often comes from boundary layer flow convergence (Fig. 14a). In the reanalysis data, there is general convergence at 850 hPa over the Central U.S., with the strongest convergence found in Oklahoma, Kansas, Arkansas, and Missouri within our budget box. Such low-level convergence in the early morning hours is mainly due to the deceleration of southerly LLJ in the region, and is further aided by enhancement to the LLJ at night due to boundary layer inertial oscillations (Blackadar 1957). The super-geostrophic nocturnal LLJ is more effective at creating horizontal flow convergence than synoptic scale LLJ that is mostly geostrophic because the latter is nearly non-divergent (Xue et al., 2018). In the WRFG simulation, the low-level convergence is weaker in the southwestern part of our budget box while the low-level flows in the northern part are mostly divergent (Fig. 14b). While the weaker low-level convergence and upper level divergence could be a result of weaker precipitation in WRFG, the former is more likely the cause of weaker locally initiated convection, because nighttime precipitation over the Central Plains is known to be forced by boundary layer convergence related to nocturnal LLJ.

For Review Only

5. Summary and conclusions

In this study, the PRISM and Stage IV precipitation data, and the NARR reanalysis data set are used to assess the performance of RCM WRFG simulation of the central U.S. wet season precipitation from 1986 to 2004. The WRFG uses the WRF model at a 50 km grid spacing with the Grell-Devenyi cumulus paramterization scheme; it is a member of the North American Regional Climate Change Assessment Program (NARCCAP). This member is chosen to detailed evaluation because WRF model is the most widely used community model for both weather prediction and regional climate simulations. It has about the largest precipitation simulation bias among the NARCCAP members over the central U.S. Great Plains. Previous studies have evaluated the NARCCAP simulations over other parts of the U.S. but less so over the Central Great Plains. In this region, significant biases are found with the precipitation simulation of WRFG. We evaluate regional atmospheric circulation and environmental condition biased in WRFG simulation to help elucidate the possible sources of its precipitation simulation error sources.

Results show that the WRFG model can generally reproduce the distribution characteristics of late spring to early summer precipitation, but it underestimates precipitation intensity in the Central Great Plains. The primary deficiency of the model in simulating the wet season precipitation over the Central Great Plains is linked to its lack of skill in simulating nocturnal precipitation. One reason is that WRFG fails to reproduce the eastward propagation of convective systems that develop in the afternoon over the Rockies, which are important contributors to the nighttime and overall precipitation over the Central Plains. This deficiency is commonly known to simulations at resolutions that require cumulus parameterization, and improvement to cumulus parameterization scheme is clearly needed for future regional climate simulations. An alternative is to perform the simulations are convection-allowing resolutions so that cumulus parameterization

For Review Only

is no longer necessary, although precipitation simulation biases may not be completely eliminated (Sun et al., 2016).

Locally developed nocturnal convection and precipitation are equally important for the Central Plains region, and such precipitation is usually forced by boundary layer convergence at the northern terminus of nocturnal boundary layer LLJ, and the LLJ also plays the important role in transporting warm and moist air from the Gulf of Mexico into the Great Plains. Hence the model's ability in accurately simulating the intensity and location of the LLJ, as well as other related environmental conditions, is another important factor to examine.

For Review Only

In WRFG simulation, it is found that on average the subtropical high over the Gulf is too weak and while the simulated pressure over western Texas is too high, leading to horizontal pressure gradient that is too weak over southern Texas, the path of warm moist air from the Gulf into the Central Great Plains. Related to this pressure pattern, the flows near the southern Texas Gulf coast show northerly anomaly (difference of simulation from reanalysis) what would act to reduce onshore moisture transport. Further, there is also northerly anomaly in west Texas. The simulated early morning LLJ is also weaker and is displaced to the east by several degrees. These differences lead to negative biases in warm moist air, hence the moist energy, transport from the Gulf into the Central Great Plains.

Low level convergence in the Central Great Plains is found to be weaker in the simulation, consistent with the weaker LLJ. The low biases in the northward synoptic scale flows on the peripheral of the subtropical high, and the low biases in the nocturnal LLJ from the South into Central Great Plains in the WRFG simulation are other important reasons of the too weak simulation of nocturnal precipitation simulation over the Central Great Plains. Reducing model error in these aspects is important; higher horizontal and vertical resolutions and improved

https://mc03.manuscriptcentral.com/aasiap

parameterization schemes including the planetary boundary layer scheme are likely needed. Spectral nudging can be used to force large scale circulations towards the reanalysis but does not solve the bias problem for future regional climate simulation if the global climate model simulation that provides the lateral boundary forcing also has the error (Hu et al., 2018). Clearly, further refinement to the WRFG RCM configurations is needed for it to be used for reliable future climate dynamic downscaling, or post-processing and calibration are needed based on the past climate simulation results. Other recent studies indicate that the lack of proper representation of topography, land-surface processes and groundwater-atmosphere interactions in models can lead to losses in soil moisture flux that reduce the MCS genesis. Such errors can be possible causes for the central Great Plains dry bias (e.g., Prein et al, 2020; Barlage et al., 2021). The deficiencies in realistically representing cloud microphysical processes and MCS kinematic properties are also among the possible causes (Wang et al. 2022). To fully understand the reasons for the biases, more numerical experiments are needed, together with detailed diagnostic analyses on the simulation results.

For Review Only

Acknowledgments. We wish to thank the NARCCAP program for providing the data which can be downloaded from https://www.earthsystemgrid.org/project/narccap.html. NARCCAP is funded by NSF, DOE, NOAA, and EPA. The NCEP Stage IV, PRISM and NARR data were downloaded, respectively, from https://www.emc.ncep.noaa.gov/mmb/ylin/pcpanl/stage4/, http://prism.oregonstate.edu and https://www.esrl.noaa.gov/psd/data/gridded/data.narr.html. The first author acknowledges the China Scholarship Council Grant that supported her visit to CAPS, University of Oklahoma, where this work was started, as part of her Ph.D. dissertation research. We also thank two anonymous reviewers whose reviews helped improve our paper.

References

Barlage, M., F. Chen, R. Rasmussen, Z. Zhang, & G. Miguez-Macho, 2021: The importance of scale-dependent groundwater processes in land-atmosphere interactions over the central United States. *Geophys. Res. Lett.*, **48**, e2020GL092171, https://doi.org/10.1029/2020GL092171.

Banacos, P. C., and D. M. Schultz, 2005: The use of moisture flux convergence in forecasting convective initiation: Historical and operational perspectives. *Weather Forecast.*, **20**, 351–366, https://doi.org/10.1175/WAF858.1.

Blackadar, A. K., 1957: Boundary layer wind maxima and their significance for the growth of nocturnal inversions. *Bull. Am. Meteorol. Soc.*, **38**, 283–290, https://doi.org/10.1175/1520-0477-38.5.283.

Bleeker, W., and M. J. Andre, 1951: On the diurnal variation of precipitation, particularly over central U.S.A., and its relation to large-scale orographic circulation systems. *Q. J. R. Meteorol. Soc.*, **77**, 260–271, https://doi.org/10.1002/qj.49707733211.

Brockhaus, P., D. Lüthi, and C. Schär, 2008: Aspects of the diurnal cycle in a regional climate model. *Meteorol. Zeitschrift*, **17**, 433–443, https://doi.org/10.1127/0941-2948/2008/0316.

Bukovsky, M. S., and D. J. Karoly, 2009: Precipitation simulations using WRF as a nested regional climate model. *J. Appl. Meteorol. Climatol.*, **48**, 2152–2159, https://doi.org/10.1175/2009JAMC2186.1.

Carbone, R. E., J. D. Tuttle, 2008: Rainfall occurrence in the U.S. warm season: The diurnal cycle. *J. Clim.*, **21**, 4132-4146, https://doi.org/10.1175/2008JCLI2275.1.

Carbone, R. E., J. D. Tuttle, D. A. Ahijevych, and S. B. Trier, 2002: Inferences of predictability

For Review Only

associated with warm season precipitation episodes. *J. Atmos. Sci.*, **59**, 2033–2056, https://doi.org/10.1175/1520-0469(2002)059<2033:IOPAWW>2.0.CO;2.

Caya, D., and R. Laprise, 1999: A semi-implicit semi-lagrangian regional climate model: The Canadian RCM. *Mon. Weather Rev.*, **127**, 341–362, https://doi.org/10.1175/1520-0493(1999)127<0341:ASISLR>2.0.CO;2.

Chen, H., T. Zhou, R. Yu, and J. Li, 2009: Summer rain fall duration and its diurnal cycle over the US Great Plains. *Int. J. Climatol.*, **29**, 1515–1519, https://doi.org/10.1002/joc.1806.

Clark, A. J., W. A. Gallus, M. Xue, and F. Kong, 2009: A comparison of precipitation forecast skill between small convection-allowing and large convection-parameterizing ensembles. *Weather Forecast.*, **24**, 1121–1140, https://doi.org/10.1175/2009WAF2222222.1.

Dai, A., F. Giorgi, and K. E. Trenberth, 1999: Observed and model-simulated diurnal cycles of precipitation over the contiguous United States. *J. Geophys. Res. Atmos.*, **104**, 6377–6402, https://doi.org/10.1029/98JD02720.

Daly, C., R. P. Nelson, and D. L. Phillips, 1994: A statistical-topographic model for mapping climatological precipitation over mountainous terrain. *J. Appl. Meteorol. Climatol.*, **33**, 140–158, https://doi.org/10.1175/1520-0450(1994)033<0140:ASTMFM>2.0.CO;2.

Davis, C.A., K. W. Manning, R. E. Carbones, S. B. Trier, and J. D. Tuttle, 2003: Coherence of warm-season continental rainfall in numerical weather prediction models. *Mon. Wea. Rev.*, **131**, 2667-2679, https://doi.org/10.1175/1520-0493(2003)131<2667:COWCRI>2.0.CO;2.

Dickinson, R. E., R. M. Errico, F. Giorgi, and G. T. Bates, 1989: A regional climate model for the western United States. *Clim. Chang.*, **15**, 383–384, https://doi.org/10.1007/BF00240465.

Diem, J. E., 2006: Synoptic-scale controls of summer precipitation in the southeastern United States. *J. Clim.*, **19**, 613–621, https://doi.org/10.1175/JCLI3645.1.

For Review Only

Gao, Y., L. R. Leung, C. Zhao, and S. Hagos, 2017: Sensitivity of U.S. summer precipitation to model resolution and convective parameterizations across gray zone resolutions. *J. Geophys. Res.*, **122**, 2714–2733, https://doi.org/10.1002/2016JD025896.

Geerts, B., and Coauthors, 2017: The 2015 plains elevated convection at night field project. *Bull. Am. Meteorol. Soc.*, **98**, 767-786, https://doi.org/10.1175/BAMS-D-15-00257.1.

Giorgi, F., M. R. Marinucci, and G. T. Bates, 1993a: Development of a second-generation regional climate model (RegCM2). Part I: Boundary-layer and radiative transfer processes. *Mon. Weather Rev.*, **121**, 2794–2813, https://doi.org/10.1175/1520-0493(1993)121<2794:DOASGR>2.0.CO;2.

——, ——, ——, and G. De Canio, 1993b: Development of a second-generation regional climate model (RegCM2). Part II: Convective processes and assimilation of lateral boundary conditions. *Mon. Weather Rev.*, **121**, 2814–2832, https://doi.org/10.1175/1520-0493(1993)121<2814:DOASGR>2.0.CO;2.

Giorgi, F., 2019: Thirty years of regional climate modeling: where are we and where are we going next? *J. Geophys. Res. Atmos.*, **124 (11)**, 5696–5723, https://doi.org/ 742 10.1029/2018JD030094.

Gochis, D. J., W. J. Shuttleworth, and Z. L. Yang, 2002: Sensitivity of the modeled North American monsoon regional climate to convective parameterization. *Mon. Weather Rev.*, **130**, 1282–1298, https://doi.org/10.1175/1520-0493(2002)130<1282:SOTMNA>2.0.CO;2.

Grell, G. A., and D. Dévényi, 2002: A generalized approach to parameterizing convection combining ensemble and data assimilation techniques. *Geophys. Res. Lett.*, **29**, https://doi.org/10.1029/2002GL015311.

Grell, G. A., J. Dudhia, and D. Stauffer, 1994: A Description of the fifth-generation Penn State /

For Review Only

NCAR mesoscale model (MM5) (No. NCAR/TN-398+STR). University Corporation for Atmospheric Research. [Available online at https://doi.org/10.5065/D60Z716B.]

Gutowski, W. J., and Coauthors, 2010: Regional extreme monthly precipitation simulated by NARCCAP RCMs. *J. Hydrometeorol.*, **11**, 1373–1379, https://doi.org/10.1175/2010JHM1297.1.

Gutowski, W. J., and Coauthors, 2020: The ongoing need for high-resolution regional climate models: Process understanding and stakeholder information. *Bull. Am. Meteorol. Soc.*, **101**, E664–E683, https://doi.org/10.1175/BAMS-D-19-0113.1.

Harding, K. J., and P. K. Snyder, 2014: Examining future changes in the character of Central U.S. warm-season precipitation using dynamical downscaling. *J. Geophys. Res. Atmos.*, **119**, 13,113-116,136, https://doi.org/doi:10.1002/2014JD022575.

Harding, K. J., P. K. Snyder, and S. Liess, 2013: Use of dynamical downscaling to improve the simulation of Central U.S. warm season precipitation in CMIP5 models. *J. Geophys. Res. Atmos.*, **118**, 12522–12536, https://doi.org/10.1002/2013JD019994.

Harris, L. M., and S. J. Lin, 2014: Global-to-regional nested grid climate simulations in the GFDL high resolution atmospheric model. *J. Clim.*, **27**, 4890–4910, https://doi.org/10.1175/JCLI-D-13-00596.1.

Helfand, H. M., and S. D. Schubert, 1995: Climatology of the simulated Great Plains low-level jet and its contribution to the continental moisture budget of the United States. *J. Clim.*, **8**, 784–806, https://doi.org/10.1175/1520-0442(1995)008<0784:COTSGP>2.0.CO;2.

Henderson, K. G., and A. J. Vega, 1996: Regional precipitation variability in the southern United States. *Phys. Geogr.*, **17:2**, 93–112, https://doi.org/10.1080/02723646.1996.10642576.

Hering, W. S., and T. R. Borden, 1962: Diurnal variations in the summer wind field over the

For Review Only

central United States. *J. Atmos. Sci.*, **19**, 81–86, https://doi.org/10.1175/1520-0469(1962)019<0081:dvitsw>2.0.co;2.

Higgins, R. W., Y. Yao, E. S. Yarosh, J. E. Janowiak, and K. C. Mo, 1997: Influence of the Great Plains low-level jet on summertime precipitation and moisture transport over the central United States. *J. Clim.*, **10**, 481–507, https://doi.org/10.1175/1520-0442(1997)010<0481:IOTGPL>2.0.CO;2.

Houze Jr., R. A., 2004: Mesoscale convective systems. *Rev. Geophys.*, **42**, RG4003, https://doi.org/doi:10.1029/2004RG000150.

Hu, X.-M., M. Xue, R. A. McPherson, E. Martin, D. H. Rosendahl, and L. Qiao, 2018: Precipitation dynamical downscaling over the Great Plains. *J. Adv. Model. Earth Syst.*, **10**, 421–447, https://doi.org/10.1002/2017MS001154.

Huang, X., C. Zhang, J. Fei, X. Cheng, J. Ding and J. Liu, 2022: Uplift mechanism of coastal extremely persistent heavy rainfall (EPHR): The key role of low-level jets and ageostrophic winds in the boundary layer, *Geophys. Res. Lett.*, **49**, e2021GL096029, https://doi.org/10.1029/2021GL096029.

Jiang, X., N. C. Lau, and S. A. Klein, 2006: Role of eastward propagating convection systems in the diurnal cycle and seasonal mean of summertime rainfall over the U.S. Great Plains. *Geophys. Res. Lett.*, **33**, 1–6, https://doi.org/10.1029/2006GL027022.

Juang, H. H., S. Hong, and M. Kanamitsu, 1997: The NCEP regional spectral model : An update. *Bull. Am. Meteorol. Soc.*, **78**, 2125–2144, https://doi.org/10.1175/1520-0477(1997)078<2125:TNRSMA>2.0.CO;2.

Kanamitsu, M., W. Ebisuzaki, J. Woollen, S.-K. Yang, J. J. Hnilo, M. Fiorino, and G. L. Potter, 2002: NCEP–DOE AMIP-II Reanalysis (R-2). *Bull. Am. Meteorol. Soc.*, **83**, 1631–1644,

For Review Only

https://doi.org/10.1175/BAMS-83-11-1631.

Katz, R. W., M. B. Parlange, and C. Tebaldi, 2003: Stochastic modeling of the effects of large-scale circulation on daily weather in the southeastern U.S. *Clim. Change*, **60**, 189–216, https://doi.org/10.1023/A:1026054330406.

Kawazoe, S., and W. J. Gutowski, 2013: Regional, very heavy daily precipitation in NARCCAP simulations. *J. Hydrometeorol.*, **14**, 1212–1227, https://doi.org/10.1175/JHM-D-12-068.1.

——, and W. J. Gutowski, 2018: Evaluation of regional very heavy precipitation events during the summer season using NARCCAP contemporary. *Int. J. Climatol.*, **38**, 832–846, https://doi.org/10.1002/joc.5412.

Kim, J., and Coauthors, 2013: Evaluation of the surface climatology over the conterminous united states in the north american regional climate change assessment program hindcast experiment using a regional climate model evaluation system. *J. Clim.*, **26**, 5698–5715, https://doi.org/10.1175/JCLI-D-12-00452.1.

Klein, S. A., X. Jiang, J. Boyle, S. Malyshev, and S. Xie, 2006: Diagnosis of the summertime warm and dry bias over the U.S. Southern Great Plains in the GFDL climate model using a weather forecasting approach. *Geophys. Res. Lett.*, **33**, 1–6, https://doi.org/10.1029/2006GL027567.

Kwon, Y. C., and S. Y. Hong, 2017: A mass-flux cumulus parameterization scheme across gray-zone resolutions. *Mon. Weather Rev.*, **145**, 583–598, https://doi.org/10.1175/MWR-D-16-0034.1.

Lavers, D.A., A. Simmons, F. Vamborg, and M. J. Rodwell, 2022: An evaluation of ERA5 precipitation for climate monitoring. *Q. J. Roy. Meteor. Soc.*, **148**, 3124–3137, https://doi.org/10.1002/qj.4351.

For Review Only

Lee, M.-I., and Coauthors, 2007a: An analysis of the warm-weason diurnal cycle over the Continental United States and Northern Mexico in general circulation models. *J. Hydrometeorol.*, **8**, 344–366, https://doi.org/10.1175/JHM581.1.

Lee, M. I., and Coauthors, 2007b: Sensitivity of horizontal resolution in the AGCM simulations of Warm season diurnal cycle of precipitation over the United States and Northern Mexico. *J. Clim.*, **20**, 1862–1881, https://doi.org/10.1175/JCLI4090.1.

Leung, L. R., and Y. Qian, 2009: Atmospheric rivers induced heavy precipitation and flooding in the western U.S. simulated by the WRF regional climate model. *Geophys. Res. Lett.*, **36**, L03820, https://doi.org/10.1029/2008GL036445.

Li, W., L. Li, R. Fu, Y. Deng, and H. Wang, 2011: Changes to the North Atlantic subtropical high and its role in the intensification of summer rainfall variability in the southeastern United States RID B-6516-2008. *J. Clim.*, **24**, 1499–1506, https://doi.org/10.1175/2010JCLI3829.1.

Liang, X. Z., L. Li, A. Dai, and K. E. Kunkel, 2004: Regional climate model simulation of summer precipitation diurnal cycle over the United States. *Geophys. Res. Lett.*, **31**, L24208, https://doi.org/10.1029/2004GL021054.

——, J. Pan, J. Zhu, K. E. Kunkel, J. X. L. Wang, and A. Dai, 2006: Regional climate model downscaling of the U.S. summer climate and future change. *J. Geophys. Res. Atmos.*, **111**, 1–17, https://doi.org/10.1029/2005JD006685.

Lim, K. S. S., S. Y. Hong, J. H. Yoon, and J. Han, 2014: Simulation of the summer monsoon rainfall over East Asia using the NCEP GFS cumulus parameterization at different horizontal resolutions. *Weather Forecast.*, **29**, 1143–1154, https://doi.org/10.1175/WAF-D-13-00143.1.

For Review Only

Lin, Y., and K. E. Mitchell, 2005: The NCEP stage II/IV hourly precipitation analyses: Development and applications. Pre- prints, 19th Conf. on Hydrology. [Available online at http://ams.confex.com/ams/ Annual2005/techprogram/paper_83847.htm.]

Loriaux, J. M., G. Lenderink, and A. P. Siebesma, 2016: Peak precipitation intensity in relation to atmospheric conditions and large-scale forcing at midlatitudes. *J. Geophys. Res. Atmos.*, **121**, 5471–5487, https://doi.org/doi:10.1002/2015JD024274.

Mearns, L. O., W. Gutowski, R. Jones, R. Leung, S. McGinnis, A. Nunes, and Y. Qian, 2009: A regional climate change assessment program for North America. *Eos, Trans. Am. Geophys. Union*, **90**, 311, https://doi.org/10.1029/2009EO360002.

Mearns, L. O., and Coauthors, 2012: The north american regional climate change assessment program overview of phase i results. *Bull. Am. Meteorol. Soc.*, **93**, 1337–1362, https://doi.org/10.1175/BAMS-D-11-00223.1.

Mesinger, F., and Coauthors, 2006: North American regional reanalysis. *Bull. Am. Meteorol. Soc.*, **87**, 343–360, https://doi.org/10.1175/BAMS-87-3-343.

Molinari, J., and M. Dudek, 1992: Parameterization of convective precipitation in mesoscale numerical models: a critical review. *Mon. Weather Rev.*, **120**, 326–344, https://doi.org/10.1175/1520-0493(1992)120<0326:POCPIM>2.0.CO;2.

Nakicenovic et al., 2000: Special Report on Emissions Scenarios. *A Special Report of Working Group III of the Intergovernmental Panel on Climate Change*. Cambridge University Press: Cambridge. 599 pp.

Nelson, B. R., O. P. Prat, D.-J. Seo, and E. Habib, 2016: Assessment and implications of NCEP Stage IV quantitative precipitation estimates for product intercomparisons. *Weather Forecast.*, **31**, 371–394, https://doi.org/10.1175/WAF-D-14-00112.1.

For Review Only

Ortegren, J. T., and Coauthors, 2011: Ocean–ttmosphere influences on low-frequency warm-season drought variability in the Gulf Coast and southeastern United States. *J. Appl. Meteorol. Climatol.*, **50**, 1177–1186, https://doi.org/10.1175/2010JAMC2566.1.

Pan, Z., J. H. Christensen, R. W. Arritt, W. J. Gutowski, E. S. Takle, and F. Otieno, 2001: Evaluation of uncertainties in regional climate change simulations. *J. Geophys. Res. Atmos.*, **106**, 17735–17751, https://doi.org/10.1029/2001JD900193.

Pauluis, O., A. Czaja, and R. Korty, 2008: The global atmospheric circulation on moist isentropes. *Science*, **321**, 1075–1079, https://doi.org/DOI: 10.1126/science.1159649.

Pitchford, K. L., and J. London, 1962: The low-level jet as related to nocturnal thunderstorms over midwest United States. *J. Appl. Meteorol.*, **1**, 43–47, https://doi.org/10.1175/1520-0450(1962)001<0043:TLLJAR>2.0.CO;2.

Pope, V. D., M. L. Gallani, P. R. Rowntree, and R. A. Stratton, 2000: The impact of new physical parametrizations in the Hadley Centre climate model: HadAM3. *Clim. Dyn.*, **16**, 123–146, https://doi.org/10.1007/s003820050009.

Prein, A.F., C. Liu, K. Ikeda et al, 2020: Simulating North American mesoscale convective systems with a convection-permitting climate model. *Clim. Dyn.*, **55**, 95–110, https://doi.org/10.1007/s00382-017-3993-2.

Qiao, F., and X. Z. Liang, 2015: Effects of cumulus parameterizations on predictions of summer flood in the Central United States. *Clim. Dyn.*, **45**, 727–744, https://doi.org/10.1007/s00382-014-2301-7.

Riley, G. T., M. G. Landin, and L. F. Bosart, 1987: The diurnal variability of precipitation across the central Rockies and adjacent Great Plains. *Mon. Weather Rev.*, **115**, 1161–1172, https://doi.org/10.1175/1520-0493(1987)115<1161:TDVOPA>2.0.CO;2.

For Review Only

Stahle, D. W., and M. K. Cleaveland, 1992: Reconstruction and Analysis of Spring Rainfall over the Southeastern U.S. for the Past 1000 Years. *Bull. Am. Meteorol. Soc.*, **73**, 1947–1961, https://doi.org/10.1175/1520-0477(1992)073<1947:RAAOSR>2.0.CO;2.

Sun, X., M. Xue, J. Brotzge, R. A. McPherson, X.-M. Hu, and X.-Q. Yang, 2016: An evaluation of dynamical downscaling of central plains summer precipitation using a WRF-based regional climate model at a convection-permitting 4km resolution. *J. Geophys. Res. Atmos.*, **121**, 13,801–13,825, https://doi.org/10.1002/2016JD024796.

Tang, Y., S. Zhong, J. A. Winker, and C. K. Walters, 2016: Evaluation of the southerly low-level jet climatology for the central United States as simulated by NARCCAP regional climate models. *Int. J. Climatol.*, **36**, 4338–4357, https://doi.org/10.1002/joc.4636.

Tapiador, F. J., A. Navarro, R. Moreno, J. L. Sánchez, and E. García-Ortega, 2020: Regional climate models: 30 years of dynamical downscaling. *Atmos. Res.*, **235**, Art. 104785, https://doi.org/10.1016/j.atmosres.2019.104785.

Tian, B., I. M. Held, N. C. Lau, and B. J. Soden, 2005: Diurnal cycle of summertime deep convection over North America: A satellite perspective. *J. Geophys. Res. D Atmos.*, **110**, 1–10, https://doi.org/10.1029/2004JD005275.

——, and Coauthors, 2017: Development of a model performance metric and its application to assess summer precipitation over the U.S. great plains in downscaled climate simulations. *J. Hydrometeorol.*, **18**, 2781–2799, https://doi.org/10.1175/JHM-D-17-0045.1.

Trier, S. B., S. D. Kehler, and J. Hanesiak, 2020: Observations and simulation of elevated nocturnal convection initiation on 24 June 2015 during PECAN. *Mon. Weather Rev.*, **148**, 613–635, https://doi.org/10.1175/MWR-D-19-0218.1.

Wallace, J. M., 1975: Diurnal variations in precipitation and thunderstorm frequency over the

For Review Only

Conterminous United States. *Mon. Weather Rev.*, **103**, 406–419, https://doi.org/10.1175/1520-0493(1975)103<0406:DVIPAT>2.0.CO;2.

Wang, S.-Y., and T.-C. Chen, 2009: The late-spring maximum of rainfall over the U.S. Central Plains and the role of the Low-Level Jet. *J. Clim.*, **22**, 4696–4709, https://doi.org/10.1175/2009JCLI2719.1.

Wang, S., R. R. Gillies, E. S. Takle, and W. J. Gutowski, 2009: Evaluation of precipitation in the Intermountain Region as simulated by the NARCCAP regional climate models. *Geophys. Res. Lett.*, **36**, L11704, https://doi.org/10.1029/2009GL037930.

Wang, D., A. F. Prein, S. E. Giangrande, A. Ramos-Valle, M. Ge, and M. P. Jensen, 2022: Convective updraft and downdraft characteristics of continental mesoscale convective systems in the model gray zone. *J. Geophys. Res. Atmos.*, **127**, e2022JD036746, https://doi.org/10.1029/2022JD036746.

Weckwerth, T. M., and Coauthors, 2004: An overview of the international H2O Project (IHOP_2002) and some preliminary highlights. *Bull. Am. Meteorol. Soc.*, **85**, 253–278, https://doi.org/10.1175/BAMS-85-2-253.

Weckwerth, T. M., and U. Romatschke, 2019: Where, when, and why did it rain during PECAN?. *Mon. Weather Rev.*, **147**, 3557–3573, https://doi.org/10.1175/MWR-D-18-0458.1.

Weisman, M. L., W. C. Skamarock, and J. B. Klemp, 1997: The resolution dependence of explicitly modeled convective systems. *Mon. Weather Rev.*, **125**, 527–548, https://doi.org/10.1175/1520-0493(1997)125<0527:TRDOEM>2.0.CO;2.

Xue, M., X. Luo, K. Zhu, Z. Sun, and J. Fei, 2018: The controlling role of boundary layer inertial oscillations in Meiyu frontal precipitation and its diurnal cycles over China. *J. Geophys.*

For Review Only

Res. Atmos., **123**, 5090–5115, https://doi.org/10.1029/2018JD028368.

Zhu, J., and X.-Z. Liang, 2005: Regional climate model simulation of U.S. soil temperature and moisture during 1982–2002. *J. Geophys. Res.*, **110**, D24110, https://doi.org/10.1029/2005JD006472.

——, and ——, 2007: Regional climate model simulations of U.S. precipitation and surface air temperature during 1982–2002: Interannual Variation. *J. Clim.*, **20**, 218–232, https://doi.org/10.1175/JCLI4129.1.

For Review Only

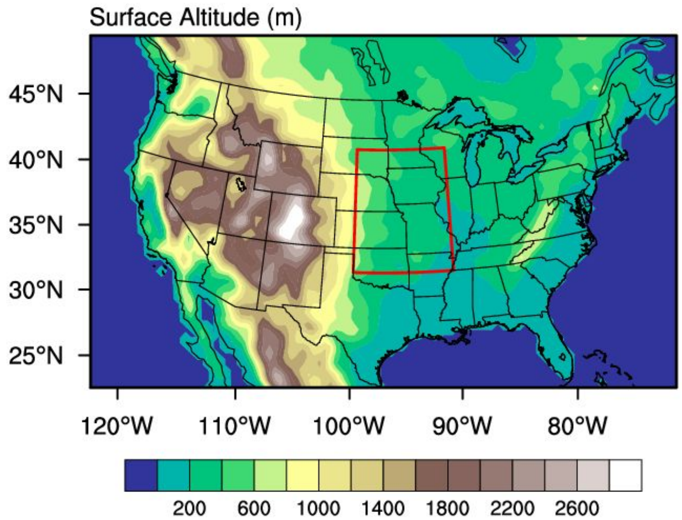

Fig. 1 Terrain elevation (m) of the United States and part of Canada from WRFG. This is part of the entire model domain which covers the conterminous United States and most of Canada. The region we focus our analyses on is the Central Great Plains enclosed by the red polygon

Review Only

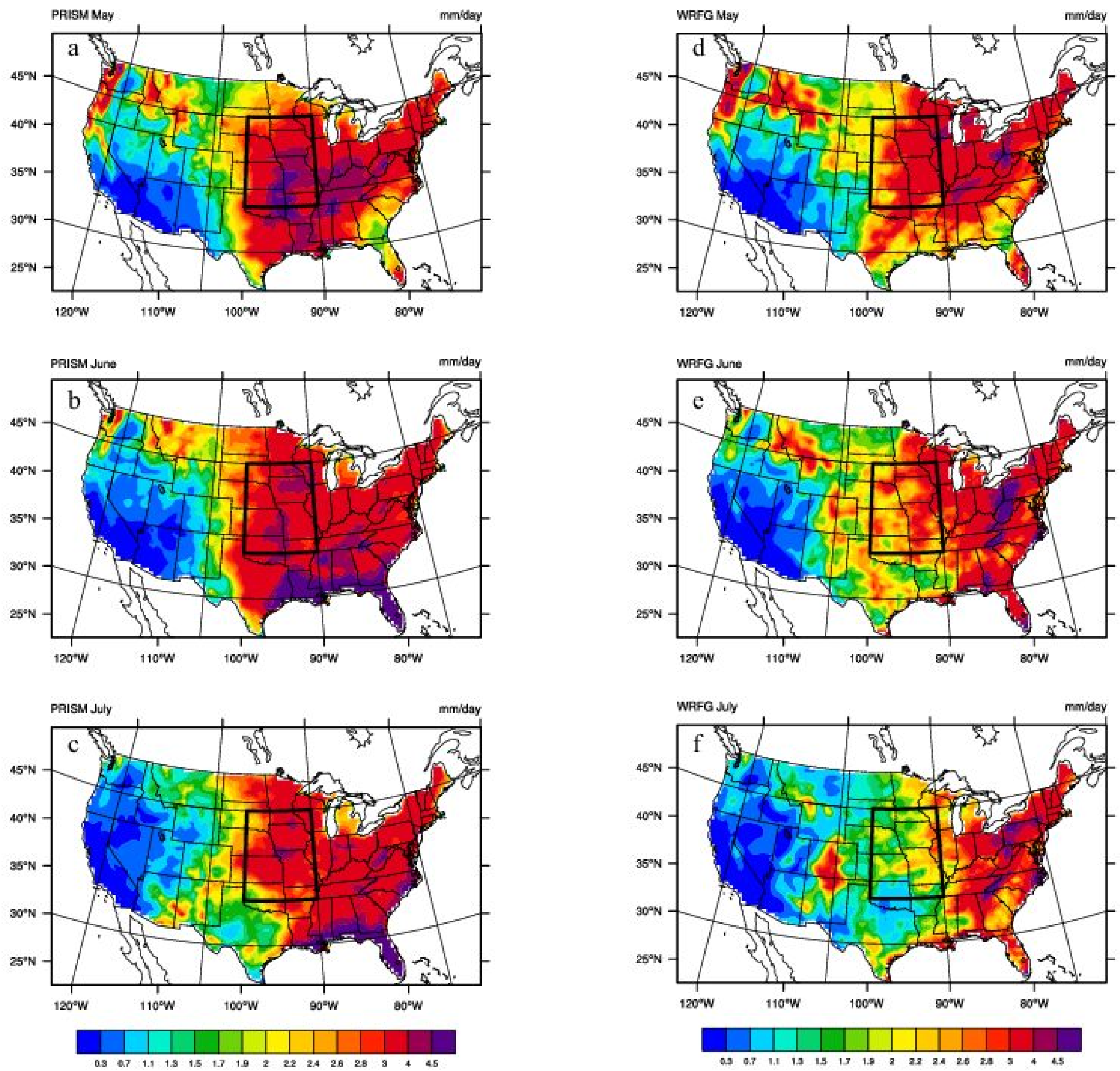

Fig. 2 Spatial distribution of daily mean precipitation intensity averaged over 1986-2004 in PRISM (a. May, b. June, c. July), and in WRFG simulation (d. May, e. June, f. July) (Unit: mm day^{-1})

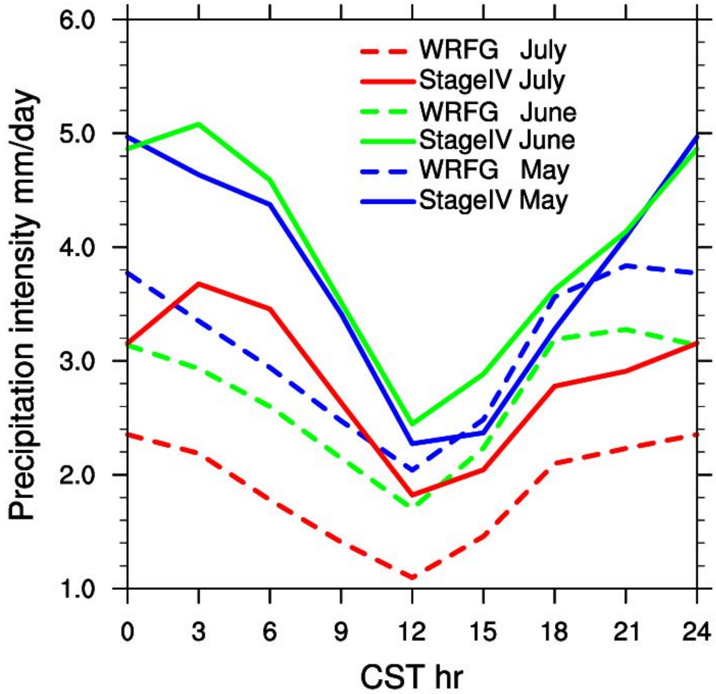

Fig. 3 Diurnal variations of mean precipitation intensity (Unit: mm day^{-1}) averaged over the central Great Plains (35-45°N, 90-100°W) in Stage IV dataset (solid line) and in WFRG simulation (dashed line) for May (Blue), June (Green) and July (Red). The mean precipitation intensities are obtained by averaging hourly accumulated precipitation over the previous three hours to the times labeled in the figure

iew Only

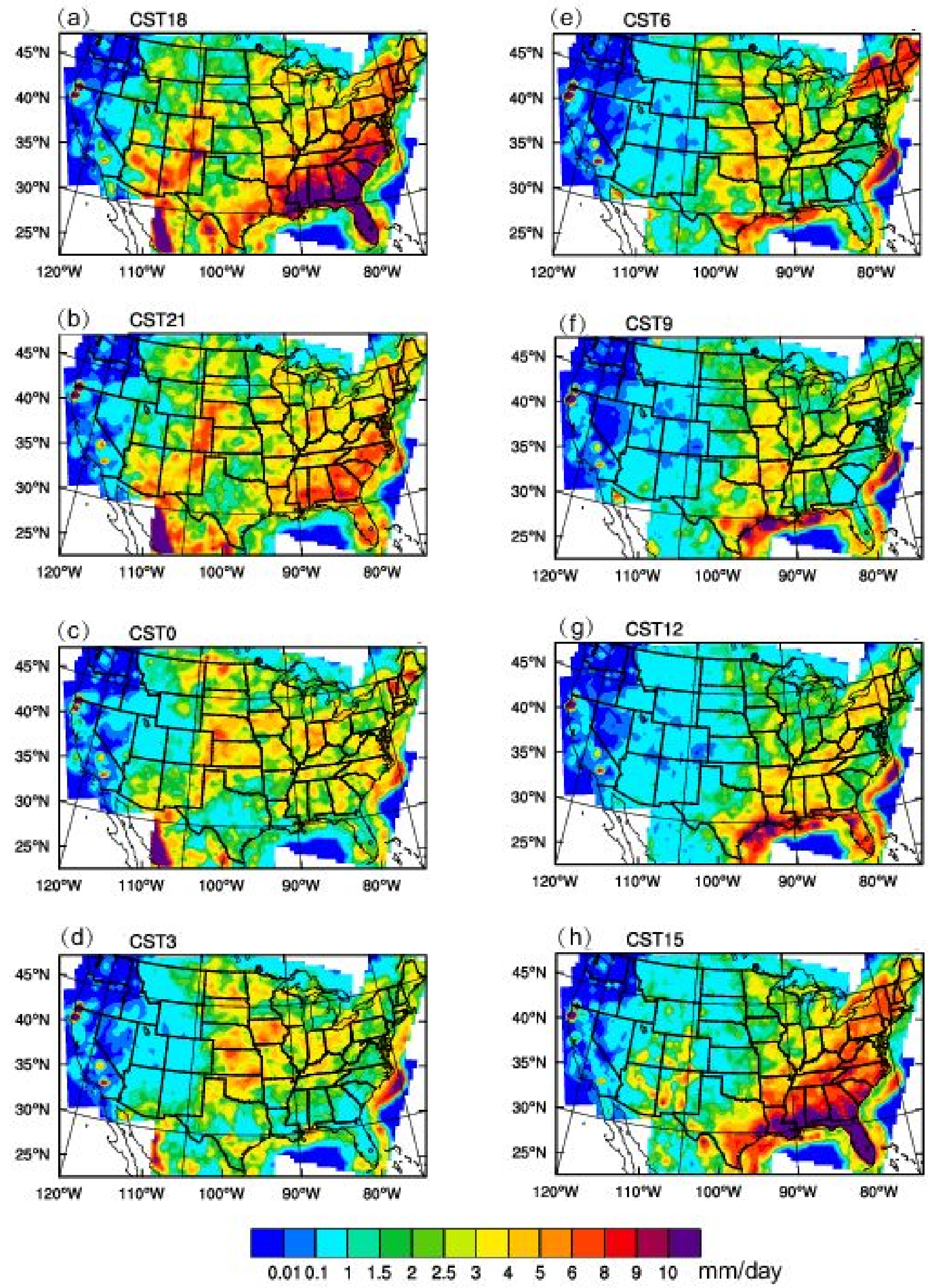

Fig. 4 Spatial distributions of precipitation intensity (Unit: mm day^{-1}) in July averaged over 2002-2015 in Stage IV data for central standard times indicated in the panels. The precipitation intensities are obtained by averaging hourly accumulated precipitation over the previous three hours to the times labeled in the figures

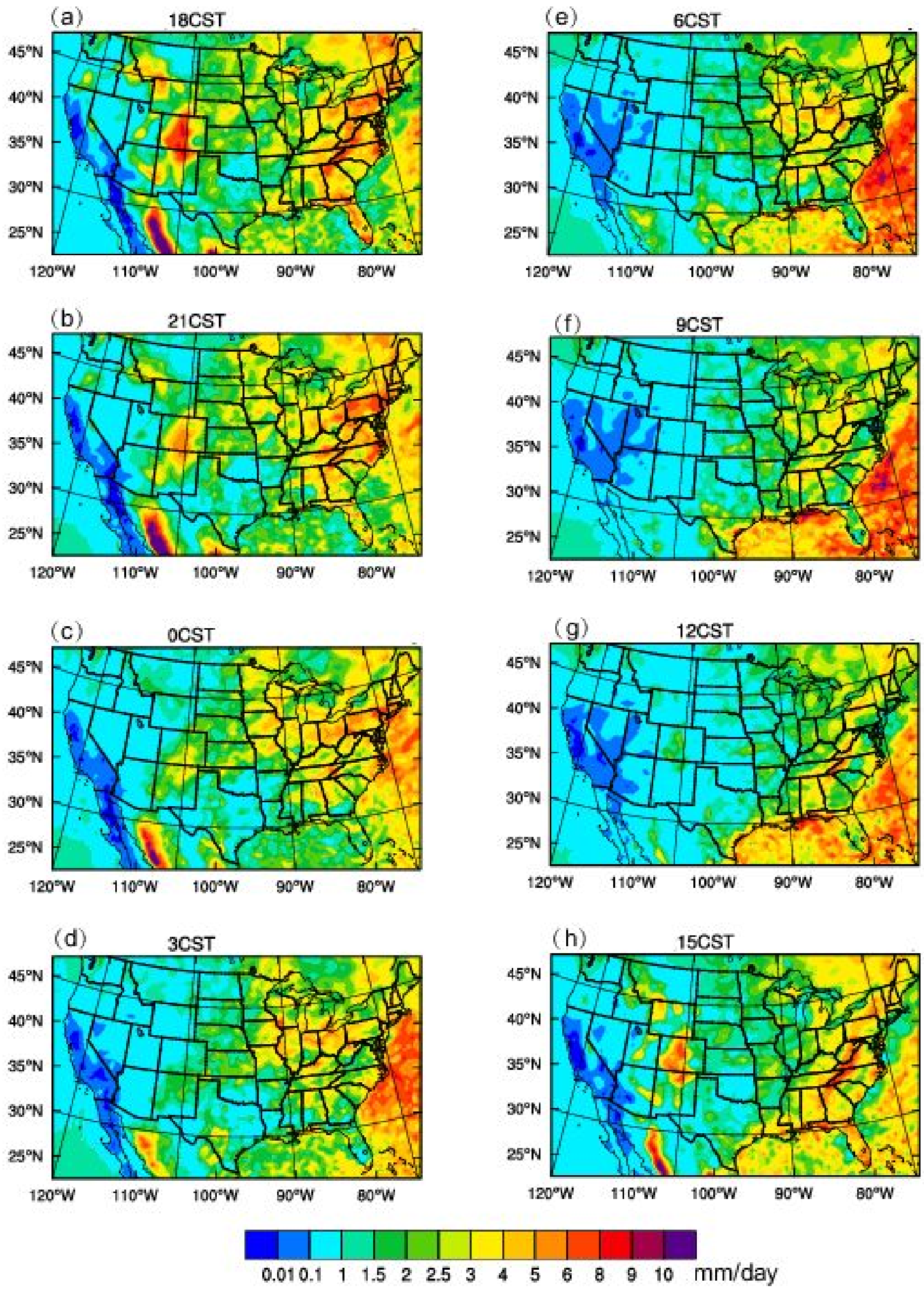

Fig. 5 Spatial distribution of precipitation intensity in July averaged over 1986-2004 in WRFG simulation (Unit: mm day^{-1})

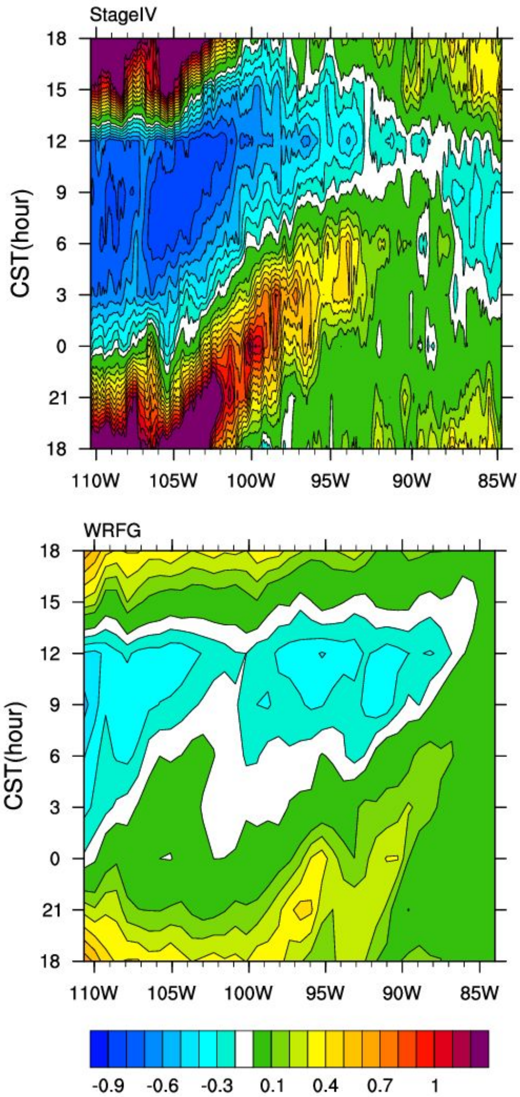

Only

Fig. 6 Hovmöller diagrams of July diurnal precipitation subtracted by and normalized by the daily mean, averaged over the 35°N-45°N latitude band, in Stage IV data (top) and precipitation simulated by WRFG (bottom)

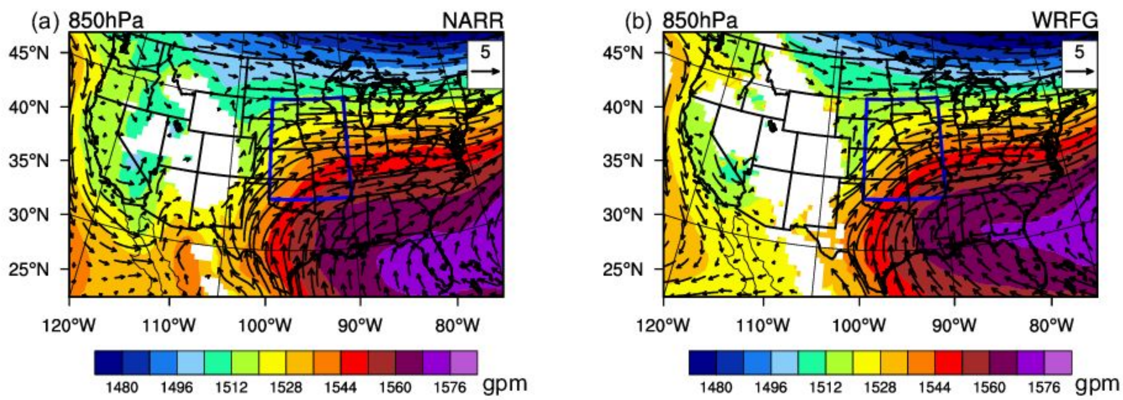

Fig. 7 The 850 hPa geopotential height (shading, unit: gpm) and horizontal wind (vector, unit: m s^{-1}) at 06 CST averaged in July over 1986-2004 in NARR reanalysis (a), and WRFG simulation (b)

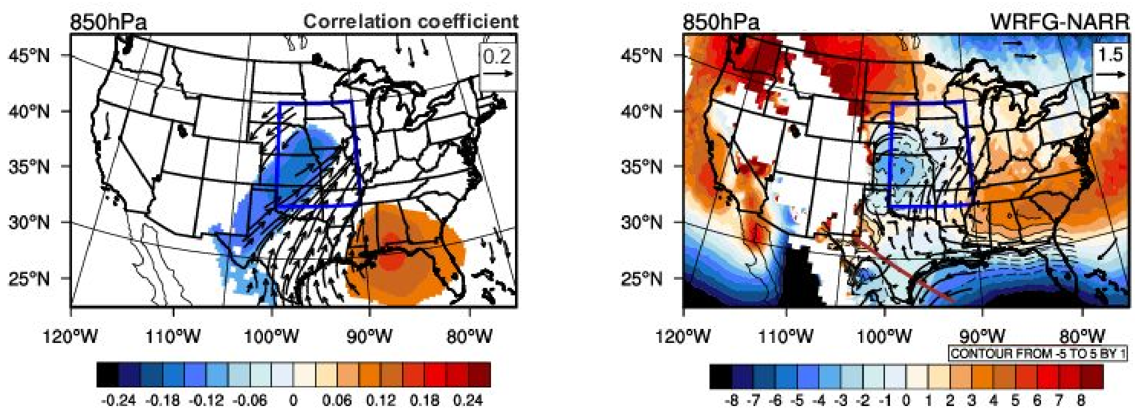

Fig. 8 The correlation coefficient of the overall Great Plains precipitation intensity within the red budget box in Fig. 1 and 850 hPa geopotential height (shading), and the correlation coefficients of 850 hPa zonal and meridional wind components with Great Plains precipitation intensity respectively (vector), significant at the 99% confidence level (a). The correlation statistics are calculated using data at 6 CST daily in July during the study period. The projection of vector in the latitudinal direction represents the correlation coefficient of zonal wind speed and precipitation intensity, and the projection of the vector in meridional direction represents the correlation coefficient of meridional wind speed and precipitation intensity. So that a long northeastward pointing vector means large positive correlations with both wind components. Difference fields between WRFG and NARR (WRFG-NARR) in 850 hPa geopotential height (shading, unit: gpm) and horizontal wind (vector, m s^{-1}) at 6 CST in July averaged over 1986-2004 (b)

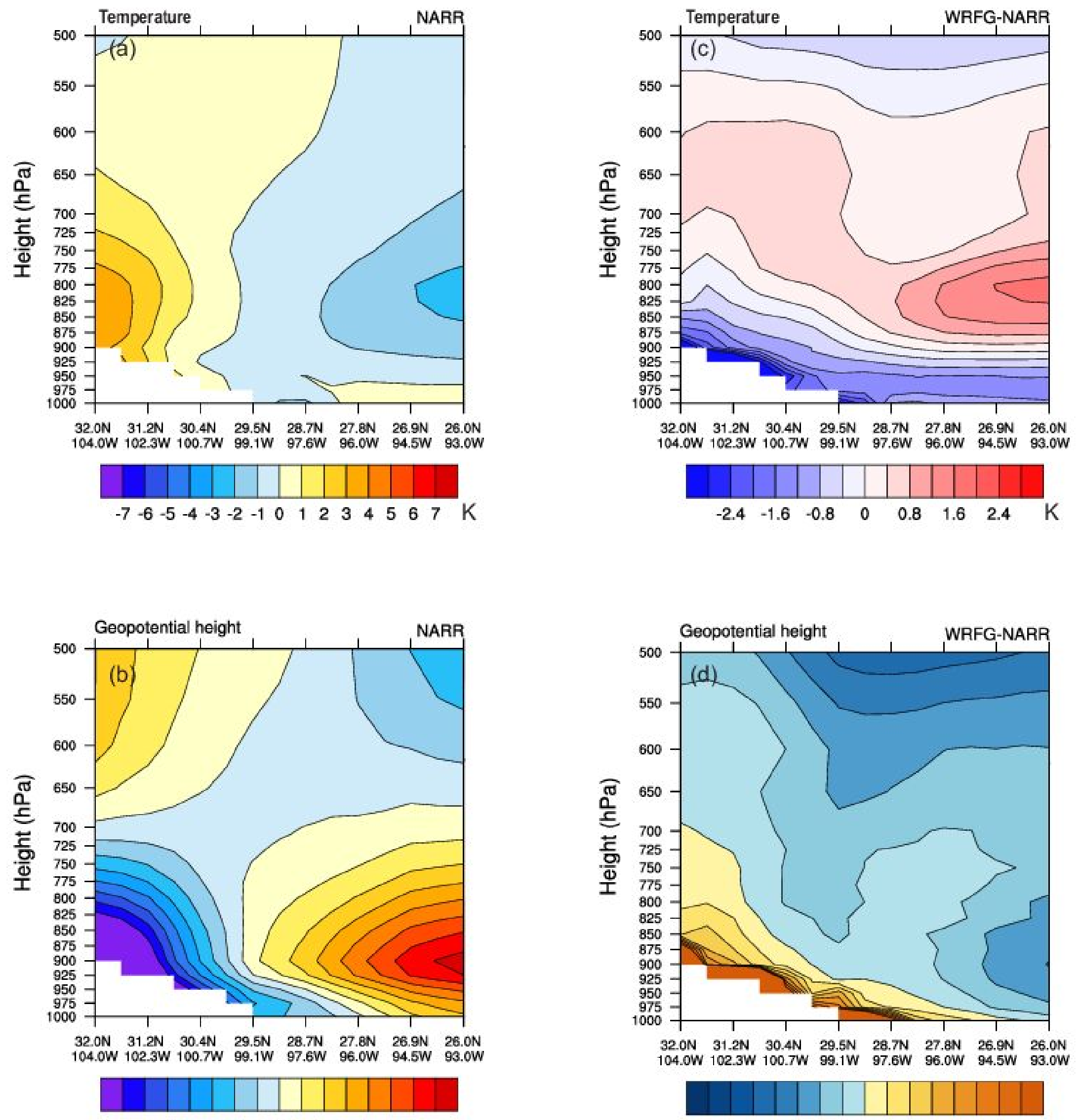

Fig. 9 Vertical cross-section of (a) NARR air temperature and (b) geopotential height with their horizontal means removed; and (c) air temperature (Unit: gpm) and (d) geopotential height difference fields between WRFG and NARR at 06 CST of July (Unit: K). The cross-section is along the northwest-southeast slope over southwestern Texas leading to the New Mexico Plateau, as denoted by the brown line in Figure 8b

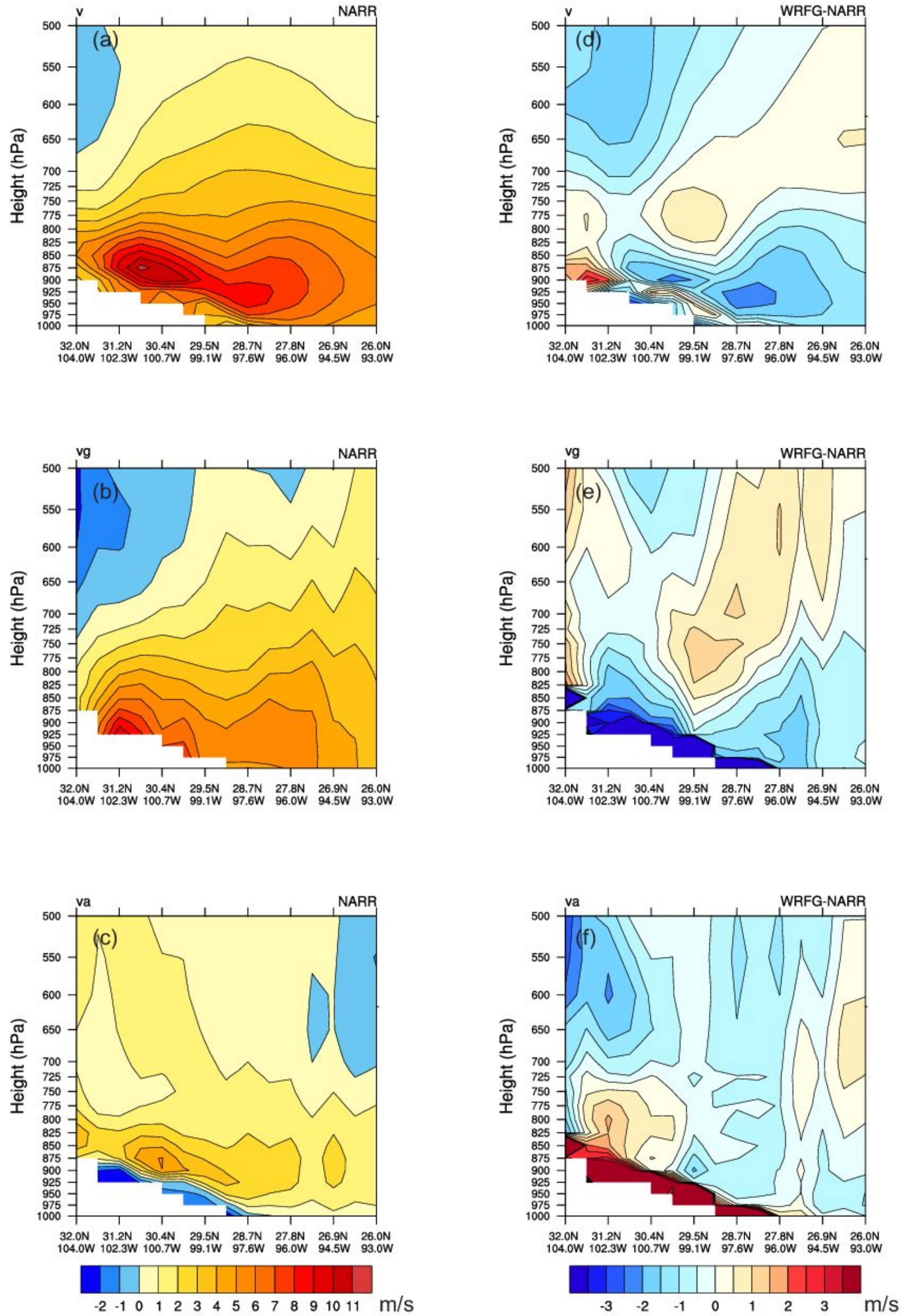

Fig. 10 Vertical cross-section along the brown line in Fig. 8b, of mean NARR (a) meridional wind, (b) meridional geostrophic wind, (c) meridional ageostrophic wind and in the right panels the corresponding difference fields between WRFG and NARR at 06 CST of July (Unit: m s^{-1})

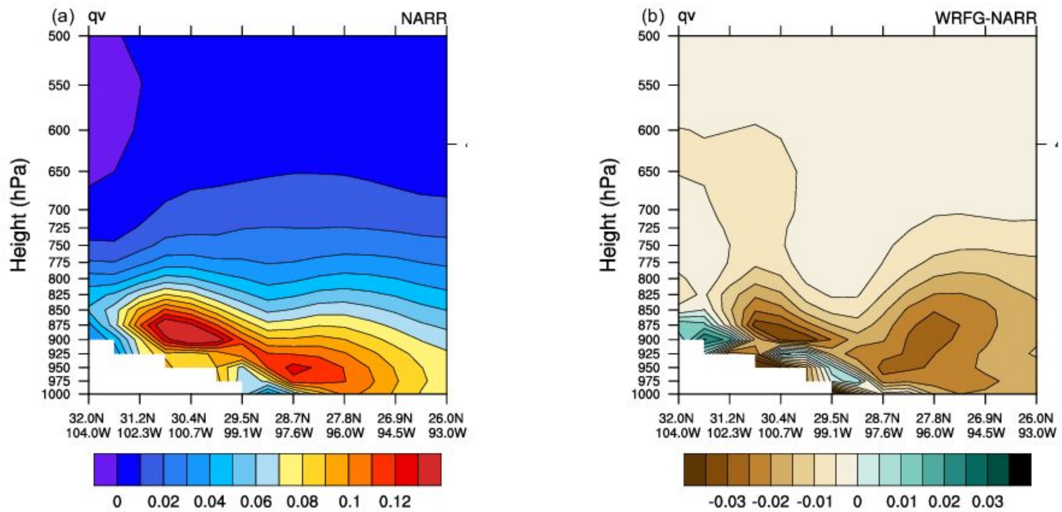

Fig. 11 Vertical cross-section of meridional moisture flux (unit: m kg kg^{-1} s^{-1}) in (a) NARR, and (b) WRFG-NARR (The cross-section is along the northwest-southeast slope which denoted by the brown line in Figure 8b.). The plotted are mean fields of 6 CST in July

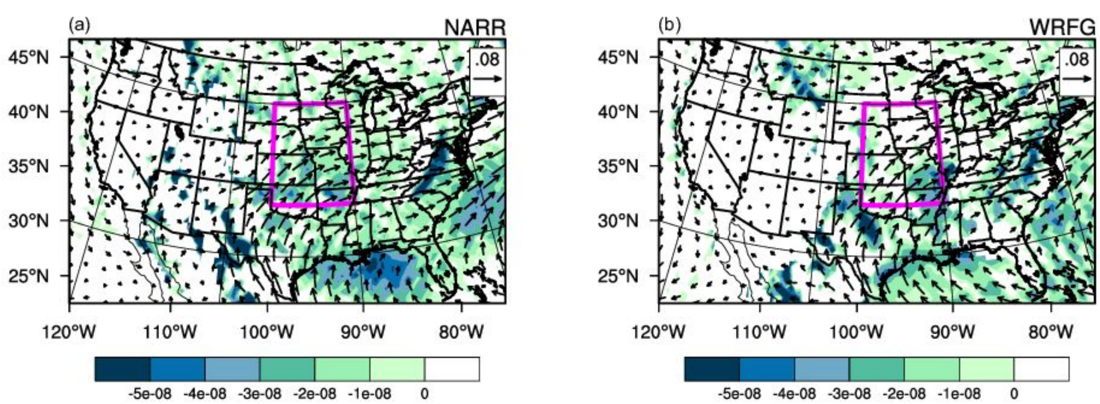

Fig. 12 Horizontal moisture flux (vector, unit: m kg kg^{-1} s^{-1}) and moisture flux divergence (shading, unit: kg kg^{-1} s^{-1}) vertically integrated from the 1000 hPa to 700 hPa in (a) NARR and (b) WRFG. The plotted are mean fields of 6 CST in July

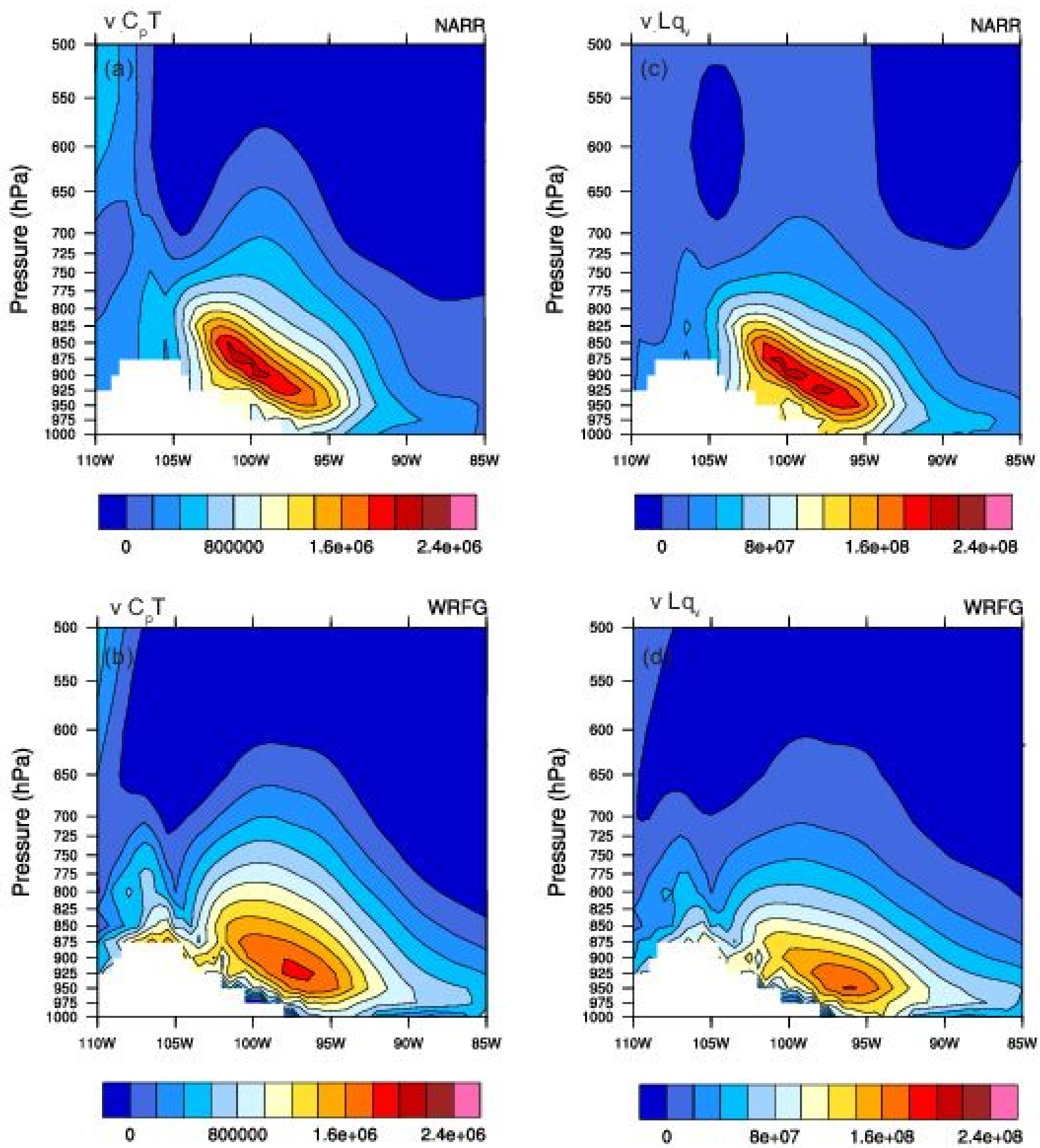

Fig. 13 Meridional sensible heat flux (unit: m J s^{-1} kg^{-1}) averaged over the 30-42.5°N latitudinal band for (a) NARR, (b) WRFG, and meridional latent heat flux (unit: m J s^{-1} g^{-1}) averaged over the 30-42.5°N latitudinal band for (c) NARR, (d) WRFG

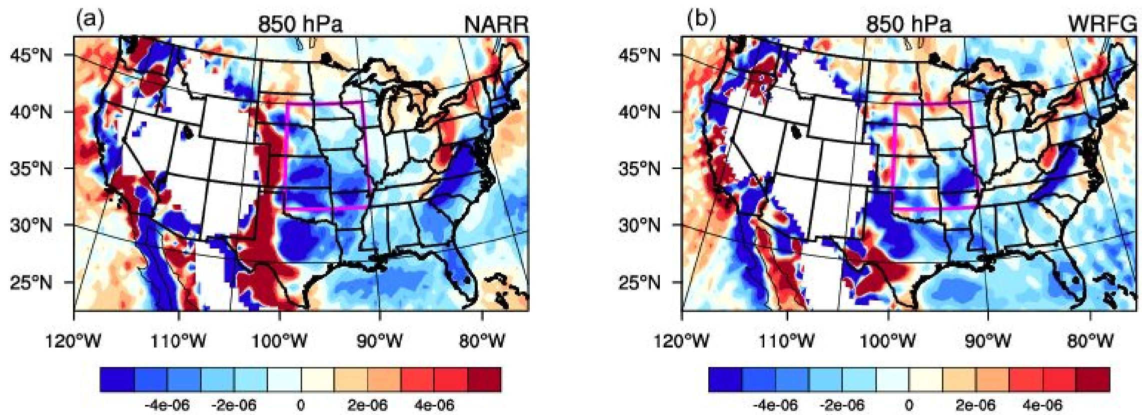

Fig. 14 Horizontal divergence at the 850 hPa level in (a) NARR, (b) WRFG (unit: s^{-1}).

For Review Only